

Light Propagation and Paired Superradiance in Coherent Medium

M. Yoshimura

Center of Quantum Universe, Faculty of Science, Okayama University,
Tsushima-naka 3-1-1, Kita-ku, Okayama, 700-8530 Japan

ABSTRACT

The problem of light propagation of frequency corresponding to half of the energy difference between a metastable excited state and the ground state of atoms is examined, and solved for coherent medium by analytic means. We demonstrate that the non-linear system of Maxwell-Bloch equation for the effective model of the Λ -type three levels is integrable in the mathematical sense. Analytic solutions thus obtained describe pulse splitting accompanied by compression, indicating a kind of non-linear instability of propagating pulses. The instability is eventually terminated by coherent two photon emission (called paired superradiance or PSR in short). These results are displayed by numerical outputs for visual understanding, as well. It is further shown that the integrable system allows a new class of soliton solutions. Solitons, implying the phenomenon of self-induced transparency at non-resonant frequencies, are stable against PSR. One of our goals of the present work is construction of a calculable theoretical framework for PSR rates associated with a trigger pulse propagation, which is achieved by combining analytic results with perturbative methods. PSR photon spectrum and its rate $\propto(\text{target number density})^2$, along with their time structure, are clarified this way. These results may open a new path for interesting technological applications such as quantum entanglement and for solving the remaining problems of the still mysterious neutrino. Some basic strategy for realistic experiments of PSR detection and soliton production is also outlined.

I Introduction

Cooperative phenomenon known as superradiance (SR) [1] may have more dramatic effects when applied to the forbidden transition: the decay rate via two photon emission may be enhanced to a macroscopic level without the wavelength restriction [2]. This is in contrast to the single photon SR enhanced decay, with the coherence region limited by the wavelength². We hereafter call the macro-coherent two photon emission [2] as paired superradiance (PSR). An example of candidate atoms for PSR is the first excited D-state of two electron system of Ba (its levels shown in Fig(1)).

In the course of establishing a firm theoretical formulation for PSR, we came across a basic reference [3] (and quite possibly many related papers unknown to the present author) in which the Maxwell-Bloch or rather a Maxwell-Schrödinger equation for an effective two level problem is derived and some numerical simulation based on this equation is performed.

The purpose of the present paper is four-fold; (1) to add to the literature of this field, fully integrated analytic solutions of the relevant non-linear system, which describe pulse splitting and compression, (2) to present a new class of soliton solutions of quantized pulse area (the terminology to be defined) that describe the phenomenon of self-induced transparency(SIT), (3) to give the PSR rate and its spectrum, both time dependent, along with its relation to soliton formation, (4) to provide the signal to the noise ratio (S/N) for radiative neutrino pair emission RNPE (a new, proposed experimental method for the precision neutrino mass spectroscopy, [4], [5]).

Our analytic solutions describe the multiple pulse splitting accompanied by compression of propagating pulses in a long target medium, when the input pulse is strong enough. The pulse strength is made quantitative by our own concept of the pulse area, a product of integrated field flux and the coupling strength to the medium. The phenomenon is a highly non-linear coherent effect of the whole system of target atoms and fields.

The multiple pulse splitting in a long target may further be interpreted as a process towards formation of many solitons, if the effect of PSR is included. Individual split pulses in medium become increasingly sharper prior to PSR. The ever sharpening pulse has an ever increasing energy density of fields and is unstable against the physical process of PSR. It must become stabilized by PSR emission, eventually resulting in formation of solitons, objects stable against PSR. This intuitive picture has been supported by extensive numerical computations performed by the present author, some of which are shown below. We would like to convince even the uneducated reader of this simple picture of what occurs in an ideal environment, the infinitely long coherent medium.

Solitons of the quantized pulse area and of arbitrary velocities have much simpler analytic forms than in the case of two level system [6]. We give explicit formulas and exhibit their pulse shape in a number of figures. Moreover, SIT occurs at non-resonant frequencies, hence might be more useful in technological applications such as communication by light and quantum entanglement: excellent candidates are ($J=0 \rightarrow J=0$) PSR transitions in alkali earth atoms.

Our general method also allows to discuss residual interaction between two solitons, which turns out attractive, suggesting existence of bound states of two solitons, presumably even a possibility of field condensate. Implication of the attractive nature of force shall be addressed in forthcoming work.

We next compute, based on perturbative methods, PSR rates in which one of the photons is the forward going pulse component. In PSR, two photons are, almost exactly, back to back emitted and have the same energy, or only this configuration in the two photon phase space is macroscopically enhanced. Calculated rates are more than adequate for detection, and even give a hope of PSR measurement in ion traps where one can expect to store a total target number of ions only as large as 10^6 .

The time structure of our triggered PSR is complicated. PSR is expected to occur rapidly and violently, most dramatically just prior to the soliton formation (and at the time of its artificial destruction). After soliton formation PSR stops, and propagating pulses become stabilized as solitons. An ideal, and our own favorite, method of observing PSR is creation of as many as possible solitons and their subsequent controlled destruction, giving the largest PSR rates at the instants of creation and destruction. We would also like to stress, for PSR detection and soliton production, great advantages of non-resonant frequency of the trigger laser, which is non-destructive to target atoms and makes experiments easier.

In any of these phenomena, irradiation of the triggering laser at the doubled wavelength is of vital importance to us, and we must fully understand the problem of light propagation in medium, which is done below. In the literature [1] that deals with SR of the two level atom, SR initiated by quantum fluctuation has extensively been discussed. The initial setting that interests us most in the present work is considerably different from this initial condition. PSR initiated by quantum fluctuation is weaker and moreover it is our main intention to utilize benefits of the triggering laser. Thus, our problem is more akin to the triggered or induced SR in the two level problem [1]. Related to this, the time delay observed in fluctuation initiated SR is absent in our triggered PSR. Despite of all these, we shall briefly mention interesting features of almost trigger-less PSR under a weaker trigger; excellent experimental signatures along with a rough estimate of its rate.

In most of our analysis below, we ignore relaxation processes, due to that the enhanced PSR is very fast: this seems a legitimate approximation under a wide range of circumstances. Moreover, the coherence we need for PSR is not a stationary state of target atoms, but rather it is a dynamically developed (with time) state of the whole system of target atoms plus fields due to the non-linear interaction between the two system. In actual experiments, the coherence is dynamically generated during a short time interval via a series of physical processes of excitation and trigger by lasers. If the time of coherence development is shorter than a typical relaxation time of relevant target state, one could achieve a well prepared state for PSR. In this sense what is needed for a positive measurement

is, in addition to the fast PSR rate, a fast preparation of coherence development, whose realization is left to a challenge for experimentalists.

At a fundamental level the soliton formation may give rise to a controlled measurement of RNPE, [4], [5], because solitons are stable against two photon emission, regarded as a crucial background to RNPE. Solitons are, on the other hand, unstable against RNPE, hence soliton formation enhances the signal to the background ratio in favor of RNPE. If the enhanced RNPE rate is larger than (spontaneous decay) rates of the next leading order QED processes (usually much smaller than 1 msec^{-1} order), then the PSR background suppressed RNPE (due to two effects discussed in the present work; mismatched trigger frequency to PSR and the soliton formation) is measurable by well controlled experiments.

The present paper is organized as a collection of (hopefully) compact sections containing many numerical outputs, and two long mathematical appendices: section headings are II Effective two level model, III Maxwell-Bloch equation and equation for the tipping angle of Bloch vector, IV Construction of analytic solutions, V Soliton solutions, VI Theory of PSR and its relation to soliton formation, VII Outlook for RNPE, VIII Appendix I Derivation of effective two level model, IX Appendix II Details towards construction of analytic solutions. We present numerical outputs, presumably more than necessary to the educated reader, to help even the uneducated reader easily understand physics behind analytic and numerical results. Appendices give some lengthy details of derivation omitted in the main body of the text.

It is hoped that this work helps experimentalists to design clever methods of detecting and measuring PSR and of creating optical soliton of our type.

Throughout this work we use the natural unit so that $\hbar = 1, c = 1$.

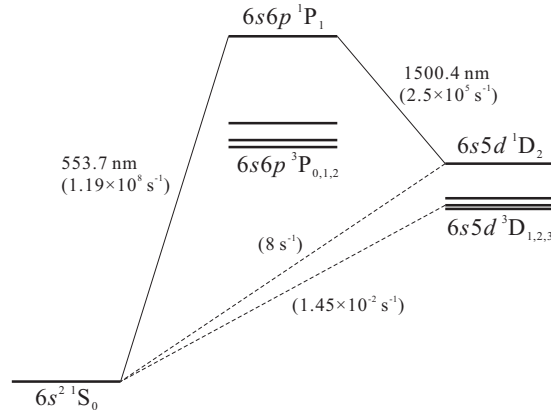


Figure 1: Λ -type low lying levels of neutral Ba atom. An excitation scheme to 1D_2 is also illustrated.

II Effective two level model

In this section we follow [3] to sketch derivation of the coupled non-linear partial differential equations of Maxwell-Bloch (MB) type, with a slight modification of notation and correction of mistakes at detuned frequencies. The essence is to derive an effective two level model for atoms of Λ -type levels such as Fig(1).

The spirit of this model is a long time average, or a truncation of past memory effects, in the sense of Markovian approximation, and slowly varying envelope approximation (SVEA). These should be an excellent approximation in our light propagation problem in medium, because this light wave at the doubled wavelength is non-resonant to target atoms, its energy being too far away from the frequency to excite to the first atomic level above the ground.

The model is summarized by the Schrödinger equation for two amplitudes of two lower levels; a S-state, 1S_0 (its amplitude given by c_g) and a D-state, 1D_2 (given by c_e) in the case of Ba atom. It has the structure of two \times two quantum system of an effective Hamiltonian \mathcal{H} ;

$$\frac{d}{dt} \begin{pmatrix} c_e \\ c_g \end{pmatrix} = -i\mathcal{H} \begin{pmatrix} c_e \\ c_g \end{pmatrix}, \quad (1)$$

$$\mathcal{H} = \begin{pmatrix} \mu_{ee}|E_0|^2 & e^{-i(2\omega-E_{eg})t}\mu_{eg}(E_0^*)^2 \\ e^{i(2\omega-E_{eg})t}\mu_{ge}E_0^2 & \mu_{gg}|E_0|^2 \end{pmatrix}. \quad (2)$$

Here $E_0(x, t)$ is the slowly varying envelope of fast oscillating field (to be multiplied by $e^{i\omega t}$). We only discuss one dimensional propagation problem, assuming the axial symmetry around the propagation axis, taken here as x -axis.

Coupling strength here is given in terms of electric (or magnetic) dipole moments between the upper level $|j\rangle$; P-states in the Ba case (the leading candidate being 1P_1), denoted by d_{je}, d_{jg} ;

$$\mu_{ee} = 2 \sum_j \frac{d_{je}^2 E_{je}}{E_{je}^2 - \omega^2}, \quad \mu_{gg} = 2 \sum_j \frac{d_{jg}^2 E_{jg}}{E_{jg}^2 - \omega^2}, \quad (3)$$

$$\mu_{eg} = \sum_j \frac{d_{je}d_{jg}}{E_c - \delta\omega}, \quad \mu_{ge} = \sum_j \frac{d_{je}d_{jg}}{E_c + \delta\omega} \quad (4)$$

$$E_c = \frac{1}{2}(E_{jg} + E_{je}), \quad \delta\omega = \omega - \frac{E_{eg}}{2}. \quad (5)$$

E1 or M1 moments d_{ji} are related to experimentally measured (or theoretically calculated in some unfortunate cases) decay rates γ_{ji} by $d_{ji}^2 = 3\pi\gamma_{ji}/E_{ji}^3$ with E_{ji} the known energy difference between two levels. Higher levels denoted by $|j\rangle$ are assumed connected to two lowest levels, $|e\rangle$ and $|g\rangle$, by strong transition elements. It would often be sufficient to consider a single level for $|j\rangle$ of strongest coupling. As explained in Appendix I, one may assume to a good approximation at $\omega \sim E_{eg}/2$ the symmetry $\mu_{eg} = \mu_{ge}$, which we take in the rest of the text.

Matrix elements in \mathcal{H} , eq.(2), of our effective Λ -model are due to the Stark effect. It is important to recognize that this shift contains two powers of propagating field E_0^2 , its absolute value being the

power or the flux of propagating field. The magnitude of Stark shift is not negligible for strong laser irradiation: two diagonal elements are of order, 6GHz for the D-state and 16 GHz for the S-state, and 2.1 GHz for the magnitude of off-diagonal elements, assuming the laser power of 10^6W mm^{-2} .

Derivation and neglected terms of this Hamiltonian structure are discussed in our Appendix I.

III Maxwell-Bloch equation and equation for the tipping angle of Bloch vector

The next step is to derive a macroscopic coupled set of equations for polarization of medium and propagating field. Throughout this work we take the continuum limit of distributed target atoms, and assume an axial symmetry around the axis of pulse propagation, which reduces our problem to $1 + 1$ (one time t and one space coordinate x) dimensional field theory. Polarization of medium is defined by a Bloch vector of 3 components (a part of density matrix elements $R_{\alpha\beta}$ in the notation of Appendix I);

$$R_1 = in(c_g^*c_e e^{i\eta} - c_e^*c_g e^{-i\eta}), \quad (6)$$

$$R_2 = -n(c_g^*c_e e^{i\eta} + c_e^*c_g e^{-i\eta}), \quad (7)$$

$$R_3 = n(|c_e|^2 - |c_g|^2), \quad (8)$$

$$\eta = (2\omega - E_{eg})t - 2kx + 2\varphi. \quad (9)$$

Here $n(x)$ is the number density of targets assumed at rest, and we took for simplicity a constant density $n(x) = n$ within a medium of finite length, $0 \leq x \leq L$. The function $\omega t - kx + \varphi(x, t)$ is the main phase part of the propagating field $e^{i\omega t} E_0$.

From the Schrödinger equation we derive the Bloch equation for polarization components,

$$\frac{\partial}{\partial t} R_1 = \frac{\mu_{ee} - \mu_{gg}}{4} |E_0|^2 R_2 + \frac{\mu_{ge}}{2} |E_0|^2 R_3, \quad (10)$$

$$\frac{\partial}{\partial t} R_2 = -\frac{\mu_{ee} - \mu_{gg}}{4} |E_0|^2 R_1, \quad (11)$$

$$\frac{\partial}{\partial t} R_3 = -\frac{\mu_{ge}}{2} |E_0|^2 R_1. \quad (12)$$

From this set of equations one has a conservation of the magnitude of the Bloch vector,

$$\frac{\partial}{\partial t} (R_1^2 + R_2^2 + R_3^2) = 0, \quad (13)$$

hence $\vec{R}^2(x, t)$ is time independent, which can be taken the squared number density $n^2(x)$.

A linear combination of R_2 and R_3 ,

$$R'_2 = \frac{R_2 - \gamma R_3}{\sqrt{1 + \gamma^2}}, \quad \gamma = \frac{\mu_{ee} - \mu_{gg}}{2\mu_{ge}}, \quad (14)$$

is conserved in our system of differential equations, and one may set this vanishing without any loss of generality, giving the condition $R_2 = \gamma R_3$. The Bloch equation is thus effectively reduced to

$$\frac{\partial}{\partial t} R_1 = \frac{\mu_{ge}}{2} (1 + \gamma^2) |E_0^2| R_3, \quad (15)$$

$$\frac{\partial}{\partial t} R_3 = -\frac{\mu_{ge}}{2} |E_0^2| R_1, \quad (16)$$

with a constant of motion, $R_1^2 + (1 + \gamma^2) R_3^2 = n^2(x)$. For the Ba D-state, $|\gamma| \sim 2.3$.

Strictly, the Bloch vector has 4 components, but to a good approximation the other component is time independent. We shall ignore this complication, relegating some explanation to Appendix I.

To proceed further, it is convenient to introduce the angle function $\theta(x, t)$, called the tipping angle, and the constant of motion $B = \pm n(x)$ by

$$R_1 = B \sin \theta, \quad R_3 = \frac{B}{\sqrt{1 + \gamma^2}} \cos \theta. \quad (17)$$

The Bloch equation is then equivalent to a relation between θ and the field power $|E_0^2|$;

$$\partial_t \theta = \omega_R, \quad \omega_R \equiv \tilde{\mu} |E_0^2|, \quad (18)$$

$$\tilde{\mu} \equiv \frac{\sqrt{1 + \gamma^2}}{2} \mu_{ge} = \frac{1}{4} \sqrt{(\mu_{gg} - \mu_{ee})^2 + 4\mu_{ge}^2}, \quad (19)$$

with $\tilde{\mu} |E_0^2| \sim 3\text{GHz} |E_0^2| / (10^6 \text{Wmm}^{-2})$ for the Ba D-state. The tipping angle θ is thus an integrated flux of $|E_0^2|$, with a weight given by the strength of Stark shift $\tilde{\mu}$,

$$\theta(x, t) = \tilde{\mu} \int_{-\infty}^{t-x} dy |E_0^2(x, y)|. \quad (20)$$

$\theta(x, \infty)$ is called the pulse area, while $\theta(x, t)$ the area function in the present work. The relation (20), containing the squared amplitude $|E_0^2|$, is different from the corresponding one in the two level problem [1] in which the field E_0 itself appears in the integrand. As an illustration, the area $\theta(x = 3\text{cm}, t = \infty)$ is plotted as a function of input laser power in Fig(2), which we need to find out necessary power values for subsequent computations on the Ba D-state. Moreover, the pulse area of 2π is an important unit for quantized solitons, a subject fully discussed in the following sections.

It is important to distinguish two cases of different signs of the constant B . If $B = n > 0$, the population difference R_3 is positive for small θ , which means that there are more atoms in the excited state than in the ground state. If $B = -n < 0$, there are more atoms in the ground state than in the excited state. From obvious reasons, we use the terminology similar to the case of the two level problem: the terminology of amplifier is used for $B > 0$ and the absorber for $B < 0$. Needless to say, this distinction is interchanged by a redefining transformation $\theta \rightarrow \theta + \pi$. Nevertheless, it is customary to take the limit value of the tipping angle, $\theta(-\infty) \rightarrow 0$, hence we stick to this terminology.

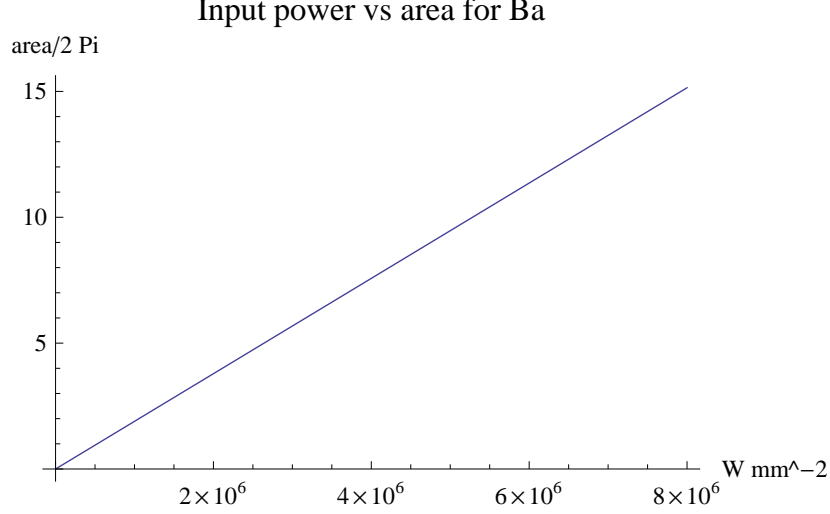


Figure 2: Pulse area of Ba D-state vs the input pulse power. Quantized areas of an integer number $\times 2\pi$ can give rise to this number of solitons. Pulse duration 3 ns assumed.

Polarization R_i of medium is related to the field E_0 by the Maxwell equation. We discuss right-moving field given by $|E_0(x, t)|e^{-i\omega(t-x)}$. Under SVEA, the evolution of envelope $|E_0(x, t)|$ is given by

$$(\partial_t + \partial_x)|E_0|^2 = \omega\mu_{ge}|E_0^2|R_1. \quad (21)$$

The coupled system of non-linear partial differential equations, eq.(15), eq.(16) and eq.(21), forms the fundamental equation of field propagation in medium, which may be called the Maxwell-Bloch equation for our effective Λ -model.

The Maxwell-Bloch equation becomes an equation for the single variable $\theta(x, t)$, using eq.(17);

$$(\partial_t + \partial_x)\partial_t\theta = \pm\alpha \sin\theta\partial_t\theta, \quad \alpha \equiv \omega\mu_{ge}n. \quad (22)$$

Our basic problem is then to solve this single, non-linear equation under an arbitrary initial and boundary data. Difference from the two level problem is in the RHS term; in the two level case there is no $\partial_t\theta$ and only term $\propto \sin\theta$, which is a potential term in the ordinary sense. This is the familiar sine-Gordon equation for propagation of pulses and SR at the resonant frequency [1].

A simplest form of relaxation may be introduced into the envelope equation (21) as a friction of the form, $\propto \kappa|E_0^2|$. This leads to a modified equation for θ ;

$$(\partial_t + \partial_x)\partial_t\theta + \kappa\partial_t\theta = \pm\alpha \sin\theta\partial_t\theta. \quad (23)$$

Both forms of equation, eq.(22) and eq.(23), may be integrated once, introducing an arbitrary function

$A(x)$ of space coordinate;

$$(\partial_t + \partial_x)\theta + \kappa\theta \pm \alpha \cos \theta = A(x). \quad (24)$$

There are more complicated forms of relaxation such as the inhomogeneous Doppler broadening in gas [7], which has to be treated separately.

When the initial data obeys the condition, $|A(x)| > \alpha$, the envelope may grow unlimitedly. This is a situation we do not discuss as our physics problem. With $|A(x)| < \alpha$, we set $A(x) = \pm\alpha \cos \theta_i(x)$. For the dissipationless case of $\kappa = 0$, the once-integrated equation becomes

$$(\partial_t + \partial_x)\theta \pm \alpha(\cos \theta - \cos \theta_i) = 0. \quad (25)$$

IV Construction of analytic solutions

It would be instructive first to discuss homogeneous solutions without spatial x dependence.

The ordinary differential equation with the simplest relaxation included is given by

$$\frac{d^2\theta}{dt^2} + (\kappa \mp \alpha \sin \theta) \frac{d\theta}{dt} = 0. \quad (26)$$

This describes a dynamical system of a fictitious pendulum (its angle location given by θ) with the friction term varying periodically with θ , $\kappa \mp \alpha \sin \theta$. There is no force acting in the ordinary sense. Equation (26) may be once integrated to give the velocity $d\theta/dt = -(\kappa\theta \pm \alpha \cos \theta)$, after a suitable redefinition of θ variable. The function of θ , $-(\kappa\theta/\alpha + \cos \theta)$, is plotted in Fig(3) for large and small frictions, to illustrate importance of the magnitude κ/α . The region of $d\theta/dt \geq 0$ alone is allowed by the energy positivity $|E_0^2| \geq 0$, and this restricts the θ region to be given by an inequality, $-(\kappa\theta + \alpha \cos \theta) \geq 0$, forming islands of θ values nearly periodically separated for small κ/α . For the dissipationless case of $\kappa = 0$, there are infinitely many pieces of such θ -islands, while these regions are limited in number for a finite κ . This dynamically allowed number of θ -islands gives the possible maximal number of produced solitons, as clarified later.

The magnitude of α for Ba is $\sim 0.72 \text{ GHz}n/(10^{16}\text{cm}^{-3})$. Smaller values of friction, e.g., less than $10^{-2}\alpha$ (the factor 10^{-2} somewhat arbitrarily chosen), imply relaxation times larger than $\sim 140 \text{ ns}$ ($n/10^{16}\text{cm}^{-3}$) $^{-1}$. We may also compare these values with the Doppler broadening in Ba gas, $\Delta_D \sim 680\text{MHz}(T/300\text{K})^{1/2}$ (with T the temperature). The requirement $\Delta_D < \alpha$ gives $T < 340\text{K}(n/10^{16}\text{cm}^{-3})^2$. We assume below that κ, Δ_D and all other relaxation rates (including those in solids) are much smaller than α , and consider the dissipationless case.

small(0.001) and large(0.01) relaxation

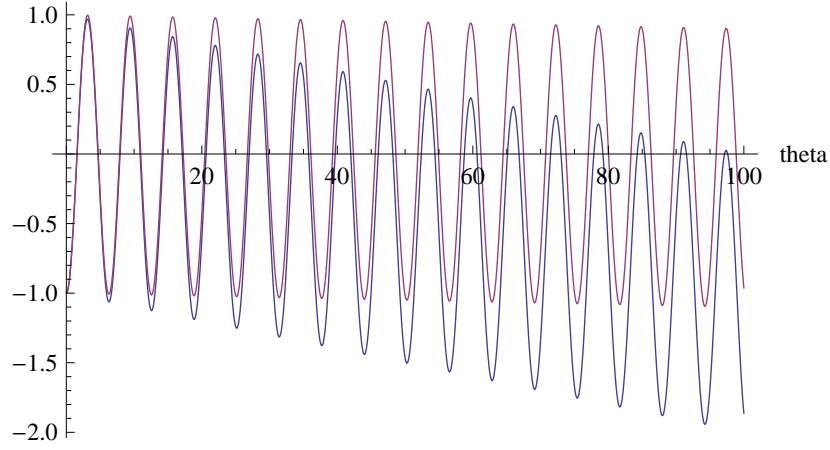


Figure 3: Allowed islands of the tipping angle given by positive ordinate values. Two choices of friction, $\kappa/\alpha = 10^{-2}$ (in blue) and 10^{-3} (in purple), are compared. Smaller frictions give more islands, giving a formation chance of more solitons.

The explicit solution without space coordinate dependence is, in the dissipationless case of $\kappa = 0$,

$$\cos \theta = -\frac{\cos \theta_0 \cosh (\alpha(t-t_0) \sin \theta_0) - 1}{\cosh (\alpha(t-t_0) \sin \theta_0) - \cos \theta_0}, \quad (27)$$

$$\omega_R = \frac{d\theta}{dt} = \frac{\alpha \sin^2 \theta_0}{\cosh (\alpha(t-t_0) \sin \theta_0) - \cos \theta_0}, \quad (28)$$

$$R_3 = -n \frac{\cos \theta_0 \cosh (\alpha(t-t_0) \sin \theta_0) - 1}{\cosh (\alpha(t-t_0) \sin \theta_0) - \cos \theta_0}. \quad (29)$$

This solution describes a dynamic motion of θ that starts from θ_0 at $t = -\infty$, reaches π at $t = t_0$, and ends finally at $2\pi - \theta_0$.

The method of deriving more general solutions of the full partial differential equation is to let parameters t_0, θ_0 here to depend on other variables of $t - x, x$. Details of this construction are given in Appendix II.

Simplest solutions that describe the initial target state either fully in the ground state (denoted by $^{(g)}$ and called the absorber) or in the excited state (denoted by $^{(e)}$ and called the amplifier) are

given by

$$|E_0^2(x, t)|^{(e)} = \frac{\epsilon_0^2(t-x)}{1 - \alpha x \sin \tilde{\theta} + (\alpha x)^2 \sin^2(\tilde{\theta}/2)}, \quad (30)$$

$$R_3^{(e)} \sim n \frac{\cos \tilde{\theta} - \alpha x \sin \tilde{\theta} + (\alpha x)^2 \sin^2(\tilde{\theta}/2)}{1 - \alpha x \sin \tilde{\theta} + (\alpha x)^2 \sin^2(\tilde{\theta}/2)}, \quad (31)$$

$$|E_0^2(x, t)|^{(g)} = \frac{\epsilon_0^2(t-x)}{1 + \alpha x \sin \tilde{\theta} + (\alpha x)^2 \sin^2(\tilde{\theta}/2)}, \quad (32)$$

$$R_3^{(g)} \sim -n \frac{\cos \tilde{\theta} + \alpha x \sin \tilde{\theta} + (\alpha x)^2 \sin^2(\tilde{\theta}/2)}{1 + \alpha x \sin \tilde{\theta} + (\alpha x)^2 \sin^2(\tilde{\theta}/2)}, \quad (33)$$

$$\tilde{\theta}(t-x) = \tilde{\mu} \int_{-\infty}^{t-x} dy \epsilon_0^2(y). \quad (34)$$

$\epsilon_0^2(t-x)$ here is the input pulse intensity.

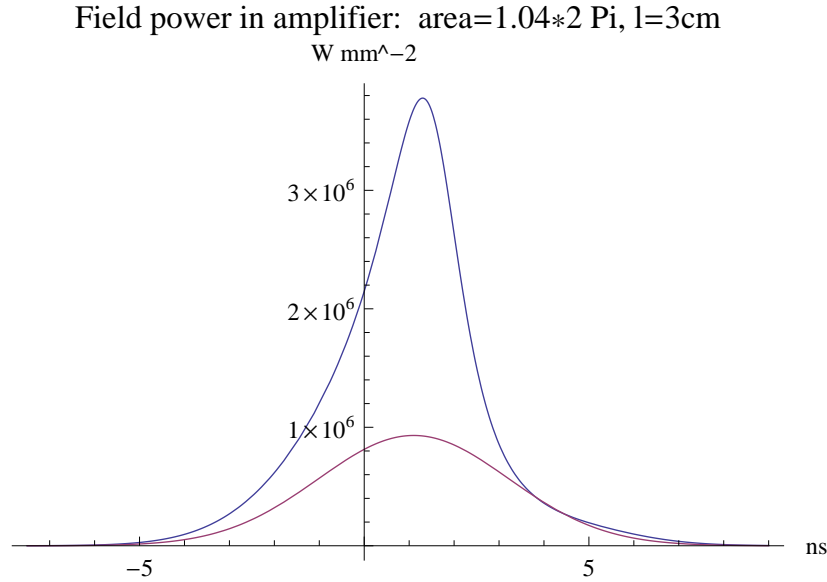


Figure 4: Compressed pulse (in blue) compared with incident pulse (in purple). The time delay (measured in difference of central locations of the two peaks) common in SR is absent here. The absolute value of abscissa coordinate is meaningless. Number density 10^{17}cm^{-3} , target length = 3 cm, laser of power $\sim 2\pi$ pulse, duration 3 ns, and the initial angle $\theta_0 = \pi/4$ are assumed.

The most general form of solutions is given in Appendix II, eq.(141) \sim eq.(142). They are written in terms of an angle factor θ_0 and the same area function $\tilde{\theta}(t-x)$ as eq.(34). The angle θ_0 describes the initial state of targets. The limit $\theta_0 \rightarrow 0$ or π , describing the fully excited or the fully ground state, gives the solutions above. A finite value of θ_0 gives a kind of the dark state [8], a measure of quantum mixture of the metastable excited and the ground state.

Field power in amplifier: area= $4.01 \times 2 \text{ Pi}$, $l=3\text{cm}$
 W mm^{-2}

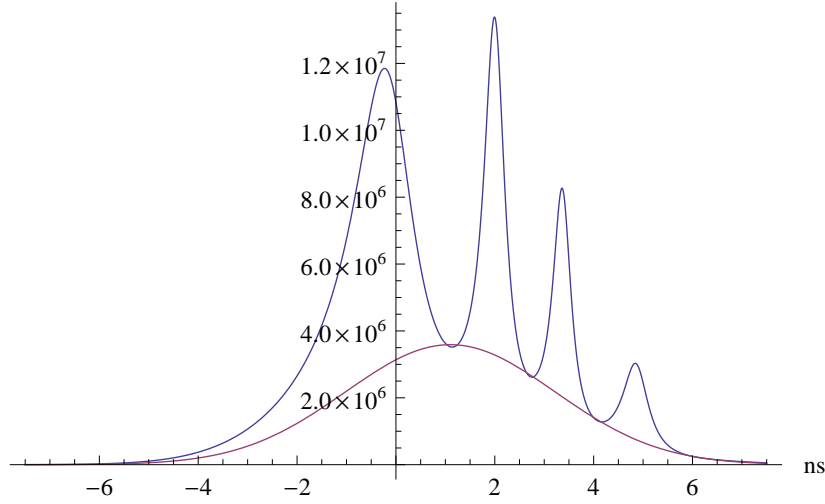


Figure 5: Multiply split pulses in medium over the entire region of incident pulse. Number density 10^{17}cm^{-3} , target length = 3 cm, laser of power $\sim 4 \times 2\pi$ pulse, duration 3 ns assumed. The initial angle $\theta_0 = \pi/4$.

Two important parameters that describe solutions of eqs.(30) ~ (34) are α and the dimensionless constant K in the area function $\tilde{\theta}$, and they are given by

$$\alpha = 3\pi \sqrt{\frac{\gamma_{je}\gamma_{jg}}{E_{je}^3 E_{jg}^3}} \frac{E_c \omega n}{E_c^2 - (\omega - E_{eg}/2)^2}, \quad (35)$$

$$K \equiv \tilde{\mu} \delta \epsilon_0^2 \sim \frac{\mu_{gg}}{4} \delta \epsilon_0^2 = \frac{3\pi}{2} \frac{\delta \gamma_{jg} \epsilon_0^2}{E_{jg}^2 (E_{jg}^2 - \omega^2)}, \quad (36)$$

where δ is the pulse duration. For the Ba D-state, they are numerically

$$\alpha \sim 0.052 \text{cm}^{-1} \frac{n}{10^{16} \text{cm}^{-3}} \frac{1.53\omega}{1.53^2 - (\omega - 0.707)^2}, \quad (37)$$

$$K \sim 18 \frac{\delta}{\text{ns}} \frac{\text{eV}^2}{2.24^2 - \omega^2} \frac{\epsilon_0^2}{10^6 \text{Wmm}^{-2}}, \quad (38)$$

with ω to be given in the eV unit.

For targets of short length, we may globally characterize the pulse modification in terms of the gain and the loss. Relative to the input pulse power (irradiated at $x = 0$) the transmitted pulse at the end of target (placed at $x = L$) has the gain or loss factor,

$$\frac{1}{1 \pm \alpha L \sin \tilde{\theta} + (\alpha L)^2 \sin^2 \tilde{\theta}/2}. \quad (39)$$

We may think of sufficiently short pulse so that remaining polarization and field inside the target is effectively described by those values at an infinite time. The area function $\tilde{\theta}(y)$ is then replaced by

its value at time infinity $\tilde{\theta}(\infty) \equiv \theta_\infty$, hence the input pulse area

$$\theta_\infty = \tilde{\mu} \int_{-\infty}^{\infty} dy \epsilon_0^2(y), \quad (40)$$

may be used. The gain or the loss factor of the transmitted pulse is thus given by

$$G \sim \frac{1}{1 \pm \alpha L \sin \theta_\infty + (\alpha L)^2 \sin^2 \theta_\infty / 2}. \quad (41)$$

A positive gain $G > 1$ requires, for $0 \leq \theta_\infty \leq 2\pi$,

$$\alpha L < \mp 2 \cot \frac{\theta_\infty}{2}. \quad (42)$$

For targets of longer length, the situation is more complicated: the pulse splitting occurs along with compression, as illustrated in Fig(4)~ Fig(8). Both of these phenomena may be interpreted as signatures of instability of propagating pulses in medium. Time profiles of propagating pulses, along with the incident pulse without medium effects, are shown in Fig(4) for the initial area of $\sim 2\pi$ and Fig(5) for the area $\sim 8\pi$; both close to integer multiples of the quantized unit 2π (the unit becoming important in discussion of solitons below). One does not observe delayed pulses, which might have been visible as shifts in two central peaks of pulses with and without medium. This is in contrast to the single photon SR initiated by quantum fluctuation, where the delay is universally present. If the target is long enough and the laser type is close to CW (continuous wave, and not pulse), there may be many split pulses within medium. In Fig(6) we show splitting into 8 well separated pulses. The number of separated pulses is $\sim \theta_\infty / 2\pi$. Spatial profiles vary with time, as illustrated in Fig(7). The ever sharpening pulses are observed, as shown in Fig(8), but in actual situations paired superradiance, not considered here, occurs and these sharpened pulses are expected to be rounded off by PSR and become objects close to solitons for which the pulse shape is unchanged with time.

In summary, the pulse modification is described by two parameters; $\alpha L, \theta_\infty$. The larger αL is, the larger modification occurs, while θ_∞ gives a measure of pulse splitting; the number of split pulses. In the Ba example, $\alpha L \sim 0.024nL/10^{16}\text{cm}^{-2}$ and $\theta_\infty \sim 4(\delta/\text{ns})(\epsilon_0^2/10^6\text{Wmm}^{-2})$, both at $\omega = E_{eg}/2$.

We now discuss interaction of two pulses, assuming that both pulses propagate in the same direction. The calculation is possible because we solved the one-mode basic equation in terms of arbitrary initial data which can be a sum of two pulses of well separated envelopes at initial times, one of them catching up the other. The influence of 2nd pulse on 1st pulse is determined by using the area sum of two pulses, for the case of $\theta_0 = 0$, $\tilde{\theta}_1(t-x) + \tilde{\theta}_2(t-x)$, which replaces $\tilde{\theta}(t-x)$ in the formula, eq.(30)~ (33). Suppose that two pulses are well separated by a distance X . Near the center of 1st pulse, we may take $t-x \sim 0$, then the effect of 2nd pulse is given by a pulse intensity modification factor A (to be multiplied by the energy density $\epsilon_1^2(0)$; the incident pulse intensity). This factor may be interpreted to define an effective potential V by using the relation $A = 1 - V(X)$. This is like defining the potential V of relativistic particle from the Lagrangian L ,

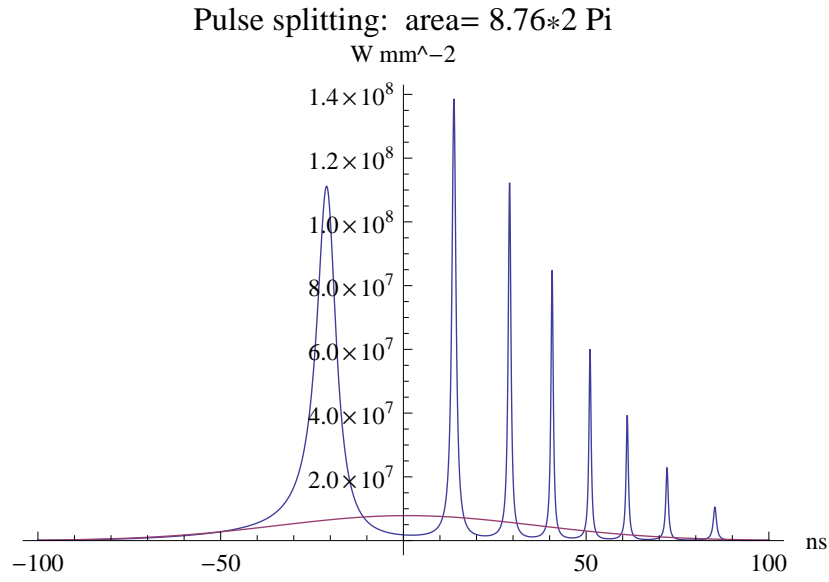


Figure 6: Splitting into many pulses in a long target. Laser (profile in purple) of intensity corresponding to $8.76 \times 2\pi$ area, time duration 50 ns and 5 GHz width is irradiated to a target of Ba number density 10^{16} cm^{-3} and length 100 cm.

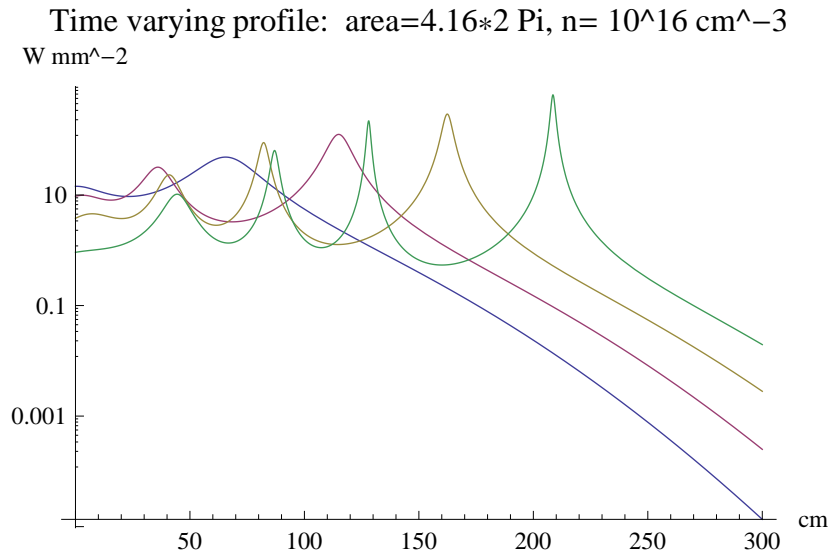


Figure 7: Time evolution of field profile at 4 different times (blue \rightarrow purple \rightarrow brown \rightarrow green in the time sequence) spaced by $0.5 \times 3 \text{ ns}$ (pulse duration), $\theta_0 = \pi/4$. Input area close to $4 \times 2\pi$ is taken.

Ever sharpening pulse: area= $1.04*2 \text{ Pi}$, $n= 10^{16} \text{ cm}^{-3}$
 $W \text{ mm}^{-2}$

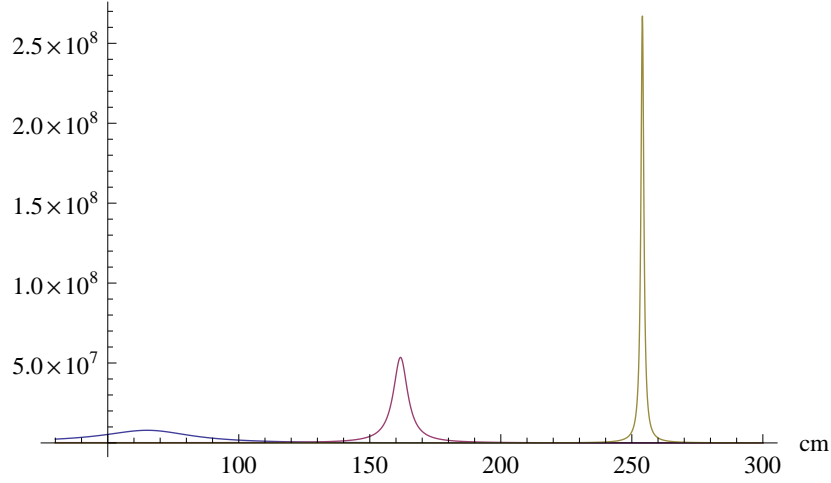


Figure 8: Ever sharpening pulse, at 3, 6, 9 ns after the pulse input.

using $L = -mc^2\sqrt{1 - \beta^2} - V$. For $\theta_0 = 0$ the potential becomes of the form (\mp corresponding to amplifier/absorber),

$$V(X) = 1 - \frac{1}{1 \mp \alpha x \sin(\tilde{\theta}_1(0) + \tilde{\theta}_2(X)) + (\alpha x)^2 \sin^2\left(\frac{\tilde{\theta}_1(0) + \tilde{\theta}_2(X)}{2}\right)}, \quad (43)$$

where x is the distance 1st pulse propagated in medium (2nd pulse is at $x - X$ in medium). This formula is of generic validity, and we shall apply it to the problem of two soliton interaction in the next section.

V Soliton solutions

Existence of stable solitons is anticipated from the topological reason when the pulse area takes quantized values of an integer times 2π . This situation is similar, but not identical, to the self-induced transparency (SIT) in the two level system [6]. In our effective Λ -model the fictitious pendulum may start from the top ($\theta = 0$) or the bottom ($\theta = \pi$), and come back to the same initial location, since its motion is limited to a single θ -island in Fig(3) between two end points (where velocity vanishes). Calculation of the pulse area for this motion gives the quantized unit of 2π .

A more physical reason for existence of solitons is that the propagating pulse in medium is not stable and becomes reshaped via splitting and compression. The sharpening process however does not last indefinitely, since the field energy density increases without bound. If the coherent region is maintained long enough, the sharpened pulse eventually emits PSR, the only possible process in our

model, thus becoming stable against PSR by formation of solitons. This picture shall be supported in conjunction with PSR rate computation in the next section.

Solitons in our effective Λ -model are solutions of

$$\partial_\eta \theta(\eta, \tau) = \mp \alpha (\cos \theta(\eta, \tau) - 1), \quad \tau = t - x, \quad \eta = x, \quad (44)$$

with the boundary condition suitable to the kink solution,

$$\theta(\eta, -\infty) = 0, \quad \theta(\eta, \infty) = 2\pi, \quad (45)$$

and a finite energy condition,

$$\int_{-\infty}^{\infty} dt (\partial_t \theta(x, t))^2 < \infty. \quad (46)$$

-(+) case in eq.(44) corresponds to amplifier(absorber). The anti-kink, or anti-soliton, does not exist, because the relevant condition, $\theta(\eta, -\infty) = 2\pi, \theta(\eta, \infty) = 0$ implying $\partial_t \theta < 0$ at some time t , is excluded from the required positivity of field energy due to $|E_0^2| \propto \partial_t \theta$.

The explicit form of the tipping angle θ and the pulse strength $|E^2|$ of soliton solutions is given in terms of a single function $T(y)$,

$$\theta(x, t) = \pm \arccos \frac{1 - \alpha^2(x - T(t - x))^2}{1 + \alpha^2(x - T(t - x))^2}, \quad (47)$$

$$\frac{\mu_{gg}}{4} |E^2(x, t)| = \pm \frac{2\alpha \partial_t T}{1 + \alpha^2(x - T(t - x))^2}. \quad (48)$$

Finiteness of energy requires a behavior of the function $T(y)$ towards \pm infinite time,

$$\int^{\infty} dy \frac{|T'(y)|}{T^2(y)} < \infty, \quad \int_{-\infty} dy \frac{|T'(y)|}{T^2(y)} < \infty. \quad (49)$$

The function $T(y)$ must be monotonic to give a positive definite flux.

A simple, linear choice of $T(\tau) \propto \tau$ gives

$$|E^2(x, t)| = \frac{2\beta v(1 - v)}{(1 - v)^2 + \alpha^2(x - vt)^2}, \quad (50)$$

$$\beta = 2 \sqrt{\frac{\gamma_{je}}{\gamma_{jg}}} \frac{E_{jg}^2 (E_{jg}^2 - \omega^2) E_c \omega n}{\sqrt{E_{je}^3 E_{jg}^3 (E_c^2 - (\omega - E_{eg}/2)^2)}}, \quad (51)$$

where α is defined by (35). The parameter v restricted to $0 < v < 1$ here may be regarded as the velocity of soliton. In the $v \rightarrow 1$ limit, soliton becomes sharpened without bound; its width $\propto 1 - v$ and its peak value $\propto 1/(1 - v)$. The integrated soliton flux is

$$\frac{2\pi v \beta}{\alpha} = \frac{4}{3} v \frac{E_{jg}^2 (E_{jg}^2 - E_{eg}^2/4)}{\gamma_{jg}} \times v \sim 4.75 \times 10^7 \text{Wmm}^{-2} \text{cm} \times v, \quad (52)$$

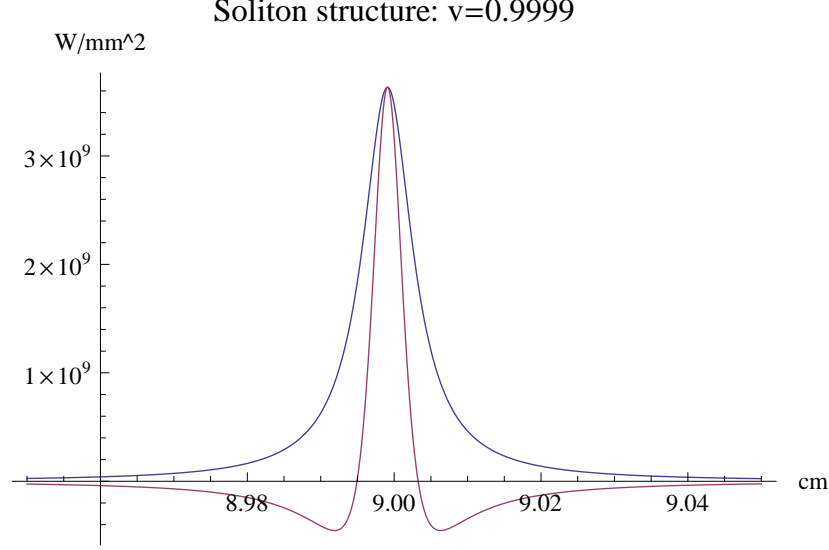


Figure 9: Soliton sandwich structure: field power and net emission rate, namely, 2 photon (emission - absorption) rate.

(numerical value for Ba), which is independent of the target number density.

Introduction of higher order powers in $T(\tau)$, like τ^3 , gives asymmetric distortion of pulses.

Fig(9) shows an example of soliton structure within target. The soliton has a sandwich structure: 2 photon emission region in the middle is surrounded by two sides of absorption region. This way the net two photon emission seen outside the target vanishes, as more fully explained in the next section on PSR rate calculation. These solitons are stable, keeping their pulse area of 2π and their shape, as illustrated in Fig(10). The soliton size is characterized by $1/\alpha$, which is $\propto 1/n$ (inversely proportional to the target number density). When the soliton propagates within medium of a different, hence mismatched number density, its shape changes, as illustrated in Fig(11).

It should be kept in mind that solitons represent, not only the field but also, the entire coherent state of atoms and fields as a whole. When a soliton exits from a target end into another region of different environment (for example, of different target number density or of different matter including vacuum), a mismatch of soliton parameters occurs and the soliton becomes destabilized and necessarily emits PSR. This gives a simple principle of detecting a soliton and PSR at the same time. An obvious obstacle against this is a fast relaxation process.

We now discuss how solitons might be dynamically created in a long target. The first step towards multiple soliton formation is to irradiate a strong pulse of area close to an integer $n \times 2\pi$ and create n number of well separated pulses. Each of these pulses are candidates of soliton of area 2π , but they must be reshaped. A method of reshaping would be to recast these pulses into an amplifier close to the ground state given by the angle $\theta_0 = \pi$. The reason for this is that at this angle value

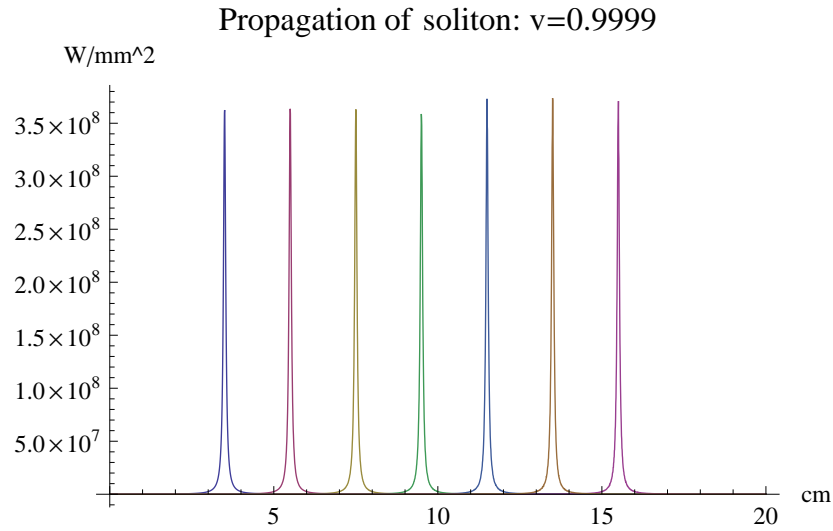


Figure 10: Spatial profile invariance of propagating soliton, shown at equally spaced different times (the first blue one giving the original pulse). Ba number density 10^{15}cm^{-3} and the velocity $0.9999 \times$ the light velocity are assumed.

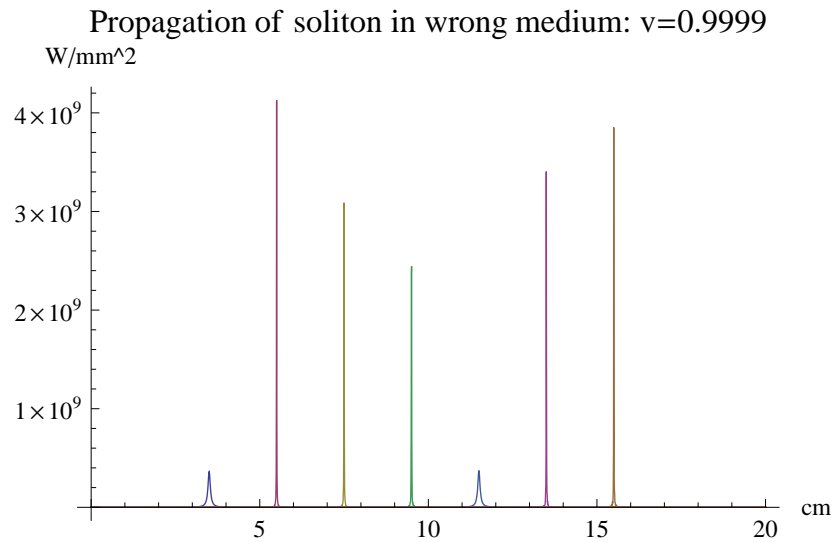


Figure 11: Spatial profiles at different times when the same soliton as in Fig(10) is put into a medium of a mismatched number density 10 times larger than in Fig(10)

the solution is given by eq.(30), thus at late times one gets

$$|E_0^2(x, t)| \sim \frac{\epsilon_0^2(t-x)}{1 - \alpha x \tilde{\delta}(t-x) + (\alpha x)^2}, \quad (53)$$

where the function $\tilde{\delta}(y)$ is the area - 2π , and $\tilde{\delta}(y) = \tilde{\theta}(y) - 2\pi \sim (\partial_y \tilde{\theta})_0 y$. This has the same form as the soliton solution, eq.(48), with $T(y) = \tilde{\delta}/(2\alpha) \sim y(\partial_y \tilde{\theta})_0/(2\alpha)$, if $\tilde{\delta}$ is small. In Fig(12) we illustrate a profile of nearly formed soliton, constructed by propagating a nearly 2π pulse in a long medium of $\theta_0 \sim \pi$. The pulse profile constructed this way is similar to, but a little bit distorted from, the soliton profile in Fig(9). The reshaping becomes perfect when the process of PSR occurs; the subject of the next section.

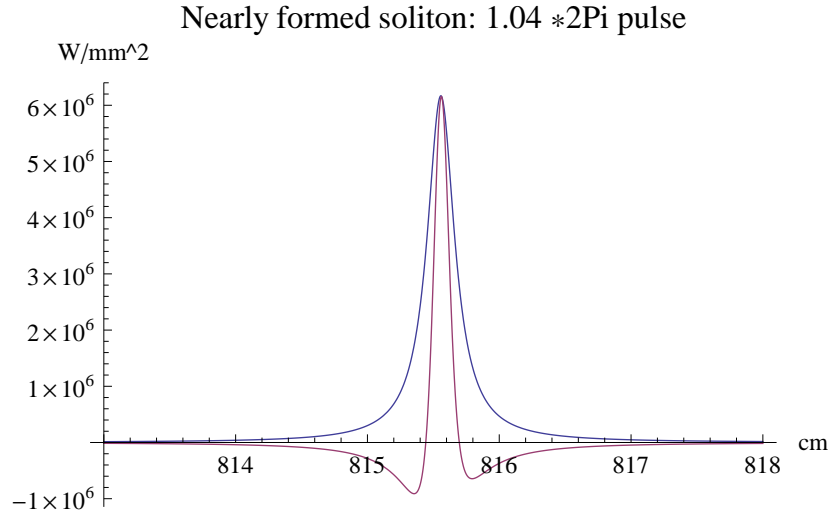


Figure 12: Spatial profile of nearly formed soliton. The net emission rate and the pulse profile after a long passage in the ground state amplifier are shown. $\theta_0 = 0.9999 \times \pi$, and Ba number density 10^{16}cm^{-3} assumed.

Two solitons infinitely separated from each other in medium propagate independently, but at finite distances they start to influence each other. Two soliton interaction of this kind is similar to the van der Waals interaction between two neutral atoms caused by induced dipoles. Interaction of two solitons may be calculated using the effective potential given by eq.(43) in the preceding section. Examples of two soliton potential are shown in Fig(13) for various target states. The conclusion on two soliton interaction is that its potential has many extremal equilibrium points for all types of target states. As the target number density increases, the depth of potential (local) minimum becomes larger and its locations becomes closer to another soliton. Implications on this force nature shall be discussed elsewhere.

2 soliton potential: absorber, amplifier and dark states

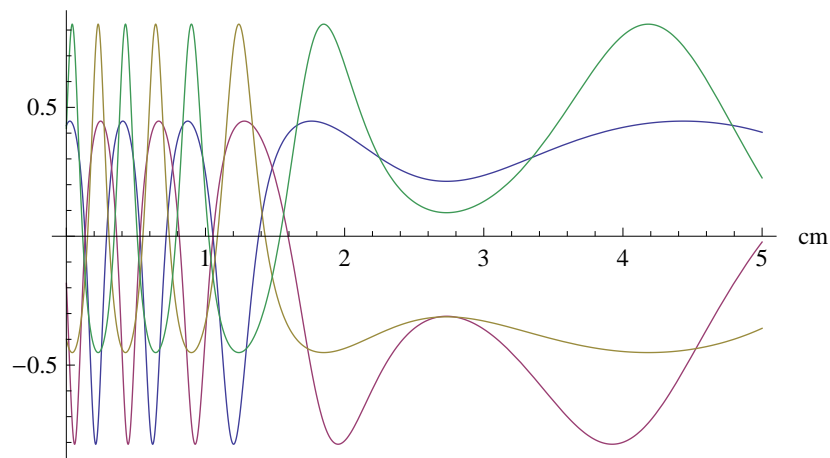


Figure 13: Effective potential between two solitons, both located in a single medium. 1st soliton of velocity $0.9 \times$ the light velocity is at 5cm away from the target end, and separated from 2nd of velocity $0.99 \times c$ by indicated distance. Ba number density $5 \times 10^{16} \text{cm}^{-3}$ is assumed, and 4 different target states, the amplifier (in blue), the absorber (purple), and two dark states (in amplifier and absorber corresponding to two signs in eqs.(141) and (142)) of $\theta_0 = \pi/2$ (green and brown) are compared.

VI Theory of PSR and its relation to soliton formation

At the outset we would like to point out that there are two kinds of PSR, the one initiated by a trigger and another that occurs without (or with a very weak) trigger, looking like a spontaneous emission at a superficial level. These may be regarded as two parts of the coherent two photon emission under an incident trigger pulse; the stimulated and the spontaneous parts. The stimulated part has a rate $\propto N_\gamma$ (the number of photons in the incident pulse), and the spontaneous part $\propto N_\gamma^0$. The rates of these two processes differ by a large factor, roughly reflecting their available number of photons; $O[|E_0(\omega)|^2/\omega]$ (the number within the trigger pulse) for the triggered PSR and $O[\omega^3/(2\pi^2)]$ (the number within a single photon phase space) for the trigger-less PSR. The spontaneous to the stimulated PSR rate ratio is numerically

$$O[10^{-4}]\left(\frac{\omega}{\text{eV}}\right)^4 \frac{10^6 \text{Wmm}^{-2}}{|E_0(\omega)|^2}. \quad (54)$$

Although its rate is smaller, there are merits for PSR without (or with a very weak) trigger; easiness of two photon simultaneous detection and the presence of the PSR time delay, which can be used as an experimental identification method for a good PSR event. It should further be noted that even a very weak trigger pulse for PSR is very useful to expedite the target coherence. An optimal and careful choice of the trigger power is obviously required.

We now discuss PSR with trigger of a larger rate. The backward photon emission in PSR is treated as perturbation to the pulse propagation. The propagation part was analyzed by Maxwell-Bloch equation and already solved. We are regarding the process as a whole single event, starting from the target triggering, coherence evolution, until PSR occurs.

Introduce a general perturbation to the propagation problem, given by a Hamiltonian \mathcal{H}_i to the effective Λ -system, which may cause a variety of transitions depending on the choice of \mathcal{H}_i ; in the case of PSR $\mathcal{H}_i = \vec{d} \cdot \vec{\epsilon}$ where $\vec{\epsilon}$ is the field of a single photon emitted in the backward direction to the pulse. For RNPE, $\mathcal{H}_i \sim G_F \nu_i^\dagger \vec{\sigma} \nu_j \cdot \vec{S}_e$ (\vec{S}_e the electron spin operator), with ν_i the neutrino field of a i -th mass eigenstate.

The interaction Hamiltonian gives rise to a perturbed amplitude of the upper level in equation for dc_e/dt , which contains the amplitude of upper level $|j\rangle$, (see eq.(88) in Appendix I). Amplitudes we need to consider in this case are the unperturbed amplitude $c_j^{(0)}(t)$ and the perturbed amplitude $\delta c_j(t)$, given respectively by

$$c_j^{(0)}(t) \sim \frac{d_{jg}}{\omega - E_{jg}} e^{-i(\omega - E_{jg})t} E^* c_g - \frac{d_{je}}{\omega + E_{je}} e^{i(\omega + E_{je})t} E c_e, \quad (55)$$

$$\delta c_j(t) \sim \frac{d_{jg}}{\omega' - E_{jg}} e^{-i(\omega' - E_{jg})t} e^* c_g - \frac{d_{je}}{\omega' + E_{je}} e^{i(\omega' + E_{je})t} e c_e. \quad (56)$$

Pulse field \times perturbed backward field contain spatial functions, $E \propto e^{-ikx}$ and $e \propto e^{-ik'x}$, where $(\omega, k), (\omega', k')$ are frequency and wave number sets of respective waves.

A crucial observation is that at the half of two level energy difference, oscillating terms have a common phase, since

$$-(\omega + E_{je}) = \omega - E_{jg}, \quad (57)$$

at $\omega = E_{eg}/2$, which much simplifies the amplitude.

We introduce a new notation for propagating and backward emitted photon fields by

$$E_0^* e^{i(\omega t - kx)} + E_0 e^{-i(\omega t - kx)}, \quad (58)$$

$$e_0^* e^{i(\omega' t - k'x)} + e_0 e^{-i(\omega' t - k'x)}, \quad (59)$$

and derive the amplitude of $|j\rangle$ -level, $c_j^{(0)}(t) + \delta c_j(t)$, by time integration, leading in the Markov approximation to

$$c_j^{(0)}(t) = -\frac{e^{iE_c t}}{E_c} \left(e^{i(\omega - \omega_0)t - ikx} E_0^* d_{je} c_e(t) + e^{-i(\omega - \omega_0)t + ikx} E_0 d_{jg} c_g(t) \right), \quad (60)$$

$$\delta c_j(t) = -\frac{e^{iE_c t}}{E_c} \left(e^{i(\omega' - \omega_0)t - ik'x} e_0^* d_{je} c_e(t) + e^{-i(\omega' - \omega_0)t + ik'x} e_0 d_{jg} c_g(t) \right), \quad (61)$$

where $\omega_0 \approx E_{eg}/2$ is the frequency of triggering pulse. Neglected terms are rapidly oscillating with x at $k' \sim -k$ (giving two counter-propagating waves).

This gives corresponding perturbation amplitudes,

$$\delta c_e(t) = ic_g(t) e^{i(k+k')x} \frac{d_{ej} d_{gj} E_0 e_0}{E_c} \frac{4 \sin(\omega + \omega' - 2\omega_0)t/2}{\omega + \omega' - 2\omega_0}, \quad (62)$$

$$\delta c_g(t) = ic_e(t) e^{-i(k+k')x} \frac{d_{ej} d_{gj} E_0^* e_0^*}{E_c} \frac{4 \sin(\omega + \omega' - 2\omega_0)t/2}{\omega + \omega' - 2\omega_0}. \quad (63)$$

One may interpret e_0 and e_0^* as annihilation and creation operators of backward emitted photons according to quantum field theory.

Equation (63) describes paired emission of two photons, counting the stimulated part of amplitude ($\propto \sqrt{N_\gamma}$) of incident pulse, and (62) describes an associated process of paired annihilation of two photons. The reason why the paired annihilation occurs is that in medium under propagating field some atoms may be in the ground state surrounded by ambient two modes of photons. This amplitude is δc_g , the perturbed ground state amplitude.

When one computes the probability of PSR, one first sums amplitudes including $e^{\pm i(k+k')x}$ over all atoms in a coherent medium. For this purpose we introduce local atomic amplitudes $c_i(x, t)$, $i = e, g$ and divide the entire coherent region $0 < x < L$ into cells of size Δx . We require $1/k \ll \Delta x \ll L$ for the cell size. Under SVEA, namely the assumption of slow variation of local amplitudes over the wavelength scale, the amplitude summation within a cell gives

$$\int_x^{x+\Delta x} dy c_i(y, t) e^{\pm i(k+k')y} \approx c_i\left(x + \frac{\Delta x}{2}, t\right) e^{\pm i(k+k')\Delta x/2} \frac{2 \sin(k+k')\Delta x/2}{k+k'}. \quad (64)$$

The last factor, when squared, gives the Dirac delta function in the form, $\Delta x 2\pi\delta(k+k')$, in the large Δx limit (of $\Delta x \gg$ the wavelength). The factor Δx in front is cancelled by the amplitude squared $|e_0|^2$ of a single backward photon.

The factor $2\pi\delta(k+k')$ implies the momentum conservation working, independently of the actual finite, but a large Δx . Our basic ansatz in the spirit of SVEA is to take for Δx its largest possible value, the target size L . Furthermore, we replace for ease of numerical computations the fast oscillating function by a more smoothly varying, yet globally correct, function;

$$\left(\frac{\sin(k+k')L/2}{k+k'}\right)^2 \rightarrow \frac{1}{(k+k')^2 + 4/(L^2)}. \quad (65)$$

We may, somewhat arbitrarily but realistically, change in rate estimates the factor L here by its fraction, which gives larger rates than given here. We may thus regard our procedure of the replacement $\Delta x \rightarrow L$ as an underestimate of more realistic rates. How much rates are underestimated actually, however, must be verified by a more laborious numerical simulation, assuming discretized sites of atoms.

Rate of the net emission $\propto R_3$ has two types of contributions; emission for $R_3 > 0$ from atoms populated more in the excited state, and absorption for $R_3 < 0$ from atoms populated more in the ground state. The absorption that occurs within target medium cannot be experimentally measured, and one measures the positive emission rate at both target ends. (If the effective rate becomes negative, no emission is measured since it means an inward emission into the target inside.) The spacetime dependence of net rates is thus given by

$$|E_0 e_0|^2 n R_3(x, t) I(x, t) \left(4 \frac{\sin(\omega + \omega' - 2\omega_0)t/2}{\omega + \omega' - 2\omega_0}\right)^2 \left(\frac{d_{ej} d_{gj}}{E_c}\right)^2 \frac{4}{(k+k')^2 + 4/(L^2)}, \quad (66)$$

where the pulse related factor $I(x, t)$ is to be given below in eq.(73). We may define the net spectral rate (net probability per unit time which can also become negative) as

$$|E_0|^2 4\pi V \omega n R_3(x, t) I(x, t) \left(\frac{d_{ej} d_{gj}}{E_c}\right)^2 \times 4 \left(\frac{\sin(\omega - \omega')L/2}{\omega - \omega'}\right)^2, \quad (67)$$

by the short time average using the well known formula,

$$\lim_{t \rightarrow \infty} \frac{4}{t} \left(\frac{\sin((\omega + \omega' - 2\omega_0)t/2)}{\omega + \omega' - 2\omega_0}\right)^2 = 2\pi\delta(\omega + \omega' - 2\omega_0). \quad (68)$$

The large time limit is valid since oscillation in time is very fast compared to polarization development under all practical situations we consider.

Convolution with the frequency distribution of the input pulse is now necessary. We assume a Gaussian power spectrum of the form,

$$F(\omega; \omega_0, \delta) = \frac{\epsilon_0^2(\omega_0)}{\sqrt{\pi}\delta} \exp\left[-\frac{(\omega - \omega_0)^2}{\delta^2}\right], \quad (69)$$

with the frequency width $\delta(= O(50 \sim 1)\text{GHz}$ for commercially available laser). The wave number integration, along with the convolution, gives

$$\int_0^\infty d\omega \int_{-\infty}^\infty dk' \frac{F(\omega; \omega_0, \delta)}{(\omega + k')^2 + 4/L^2} \delta(\omega + |k'| - E_{eg}) \sim \frac{\pi L}{2} F(E_{eg} - \omega'; \omega_0, \delta), \quad (70)$$

leading to the differential spectrum $d^2\Gamma/d\omega'dt$ (having the dimension of rate, 1/time) of the backward photon of energy ω' ;

$$8\pi^2 n^2 V (3\pi)^2 \frac{\gamma_{je}\gamma_{jg}}{E_c^2 E_{je}^3 E_{jg}^3} \frac{E_{eg}\pi}{4} \frac{E_{eg} - \omega'}{(2\omega' - E_{eg})^2 + 4/L^2} \frac{\epsilon_0^2(\omega_0) \exp[-\frac{(\omega' - E_{eg} + \omega_0)^2}{\delta^2}]}{\sqrt{\pi}\delta} \frac{\exp[-\frac{(t-x)^2}{\Delta^2}]}{\sqrt{\pi}\Delta} r_3(x, t; \omega') I(x, t; \omega'), \quad (71)$$

$$r_3(x, t; \omega') = \pm \frac{1}{\sqrt{1 + \gamma^2}} \frac{\cosh(\alpha x \sin \theta_0) \cos \theta_0 (1 - \cos \theta_0 \cos \tilde{\theta}) \pm \sinh(\alpha x \sin \theta_0) \cos \theta_0 \sin \theta_0 \sin \tilde{\theta} - (\cos \theta_0 - \cos \tilde{\theta})}{\cosh(\alpha x \sin \theta_0) (1 - \cos \theta_0 \cos \tilde{\theta}) \pm \sinh(\alpha \sin \theta_0 x) \sin \theta_0 \sin \tilde{\theta} - \cos \theta_0 (\cos \theta_0 - \cos \tilde{\theta})}, \quad (72)$$

$$I(x, t; \omega') = \frac{\sin^2 \theta_0}{\cosh(\alpha x \sin \theta_0) (1 - \cos \theta_0 \cos \tilde{\theta}) \pm \sinh(\alpha x \sin \theta_0) \sin \theta_0 \sin \tilde{\theta} - \cos \theta_0 (\cos \theta_0 - \cos \tilde{\theta})}. \quad (73)$$

For the input pulse we assumed a time structure of the Gaussian form, characterized by a width Δ and centered at $t = x$. Two cases of \mp correspond to the state of targets; absorber (amplifier).

Note that we used neither the conventional Gaussian width given by the variance, nor the half width at half its maximum. Our width is $\sqrt{2} \times$ the Gaussian and $1/\sqrt{\ln 2} \times$ the half width.

For the Ba D-state, the basic unit of differential spectrum for the target number density $n = 10^{16}\text{cm}^{-3}$ and the pulse power $\epsilon_0^2 = 10^6\text{W mm}^{-2}$ is (under the $\hbar = 1, c = 1$ unit)

$$8\pi^2 (3\pi)^2 (10^{16}\text{cm}^{-3})^2 \text{cm}^2 \text{GHz MHz } 10^6\text{W mm}^{-2} = 5.7 \times 10^{19} \text{Hz eV}, \quad (74)$$

to be multiplied by

$$\left(\frac{n}{10^{16}\text{cm}^{-3}}\right)^2 \frac{V}{\text{cm}^3} \frac{E_{eg} - \omega'}{(2\omega' - E_{eg})^2 + 4/L^2} \frac{\epsilon_0^2}{10^6\text{W mm}^{-2}} \frac{\exp[-\frac{(\omega' - E_{eg} + \omega_0)^2}{\delta^2}]}{\sqrt{\pi}\delta} d\omega' \\ \times r_3(\omega', x, t) I(\omega', x, t) \frac{\exp[-\frac{(t-x)^2}{\Delta^2}]}{\sqrt{\pi}\Delta} dt, \quad (75)$$

where all energies should be given in the eV unit. Two cases of $+(-)$ correspond to the absorber (amplifier).

The time dependence of rate $d^2\Gamma/d\omega'dt$ is due to the rapidly varying pulse shape. A more practical measure of event rate is time integrated event number per a shot of pulse;

$$\int_{-\infty}^\infty dt \frac{d^2\Gamma(\omega'; x, t)}{d\omega'dt}. \quad (76)$$

From the measurement point of view, only two locations are of practical importance; $x = 0$ the target left end for measurement of the backward emitted photon of PSR, and $x = L$ the right end for measurement of the forward emitted photon.

The frequency spectrum of backward photon is sharply peaked at the middle point of level spacing, $\omega' = E_{eg}/2$, if the trigger frequency is tuned to this value, $\omega_0 = E_{eg}/2$. A quantity of practical importance for the overall rate is the frequency integrated (time dependent) rate given by

$$\int_0^\infty d\omega' \frac{d^2\Gamma(\omega'; x, t)}{d\omega' dt} = \int_0^\infty d\omega' \frac{\exp[-\frac{(\omega' - E_{eg} + \omega_0)^2}{\delta^2}]}{\sqrt{\pi}\delta} \frac{E_{eg} - \omega'}{(2\omega' - E_{eg})^2 + 4/L^2} F(\omega'; x, t), \quad (77)$$

where $F(\omega'; x, t)$ is slowly varying in frequency ω' . We may approximate this frequency integral by taking correct behavior in the two limiting regions, $\delta L \gg 1$ and $\delta L \ll 1$, and smoothly interpolating in the interval. At the tuned point $\omega_0 = E_{eg}/2$, one may adopt the following approximation,

$$\int_0^\infty d\omega' \frac{\exp[-\frac{(\omega' - E_{eg}/2)^2}{\delta^2}]}{\sqrt{\pi}\delta} \frac{E_{eg} - \omega'}{(2\omega' - E_{eg})^2 + 4/L^2} F(\omega'; x, t) \approx \frac{\frac{E_{eg}}{2} F(\frac{E_{eg}}{2}; x, t) \sqrt{\pi} L^2}{\sqrt{\pi} + 2L\delta}. \quad (78)$$

We checked that this approximation is valid to an accuracy of $\sim 15\%$ level.

Assuming that the pulse shape variation is slow, one may introduce a slowly varying, time dependent rate by taking the short time-average and frequency-integration, to obtain a total net event number (emission - absorption event) per a shot of pulse as

$$\mathcal{N}(x, t) = 3.2 \times 10^{24} \left(\frac{n}{10^{16} \text{cm}^{-3}}\right)^2 \frac{\epsilon_0^2}{10^6 \text{Wmm}^{-2}} \frac{V}{\text{cm}^3} r_3\left(\frac{E_{eg}}{2}, x, t\right) I\left(\frac{E_{eg}}{2}, x, t\right) \frac{\sqrt{\pi} L / \text{cm}}{\sqrt{\pi} + 2L\delta}. \quad (79)$$

The last factor for the pulse duration of $\delta = 45\text{GHz}$ and $L = 3 \text{ cm}$ is ~ 0.5 .

The more effective and useful event rate (number of events per unit time) in actual experiments is given by this event number per a shot divided by the repetition cycle time τ_r of excitation and trigger. For instance, if the pulse repetition cycle τ_r is 1 msec, a practical experimental rate is $\mathcal{N}/\tau_r = 10^3 \mathcal{N}$ Hz. We caution that all event numbers shown in Fig(14) \sim Fig(23) are events per a shot of pulse, and one has to multiply $1/\tau_r$ (depending on experimental setup) for effective and more realistic rates per unit time.

We now exhibit several figures to illustrate physics of analytic results given here. These PSR rates are computed, using the rate formula and analytic solutions of the pulse propagation for r_3, I_1 . The first figure Fig(14) shows the initial angle θ_0 dependence of the backward rate (measured at $x = 0$) and the forward rate (at $x = L$). Except at soliton formation discussed later, the forward-backward asymmetry in rate is not large (typically $\leq 15\%$).

An example of Ba backward photon spectrum is shown in Fig(15). In this computation we took the Gaussian frequency distribution of input laser, its width given by 45 GHz. Both spectral shape and rate are indistinguishable up to the passage time of pulse at the target end, but the rate rapidly decreases much beyond the passage time. It thus becomes important to devise a fast recycling scheme for excitation and trigger of the target, in order not to wait for a null result.

The laser power dependence of rate is shown in Fig(16). Fig(17) shows dependence on the target number density dependence, indicating that PSR may be detectable for Ba number densities as low

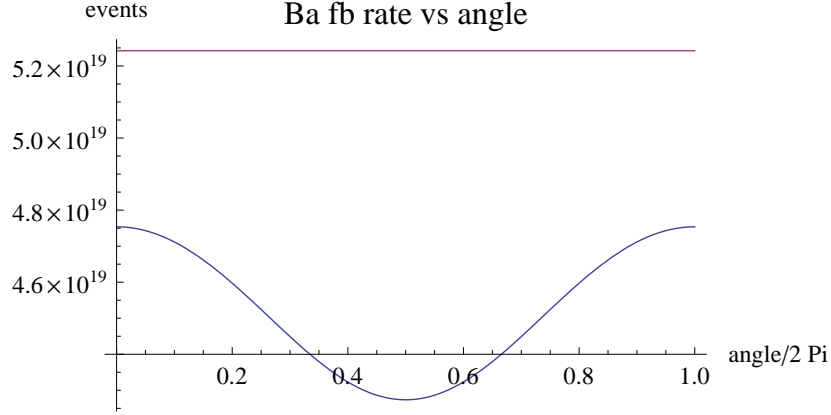


Figure 14: Angle (θ_0) dependence of forward (blue) and backward (purple) rates measured at the passage time of the target end (taken 3cm). Power 10^6W mm^{-2} , number density 10^{16}cm^{-3} , laser duration 3 ns assumed.

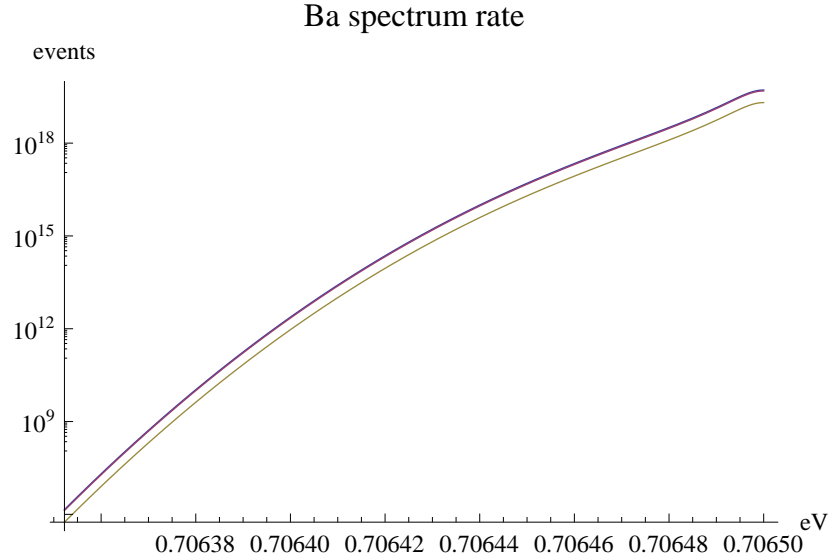


Figure 15: Spectrum rate at 3 different times, $(0.1, 1, 5) \times$ the passing time of the target end. Power 10^6W mm^{-2} , number density 10^{16}cm^{-3} , target length = 3 cm, laser duration 3 ns, $\theta_0 = \pi/4$ assumed. Rates monotonically decrease in this range of time sequence.

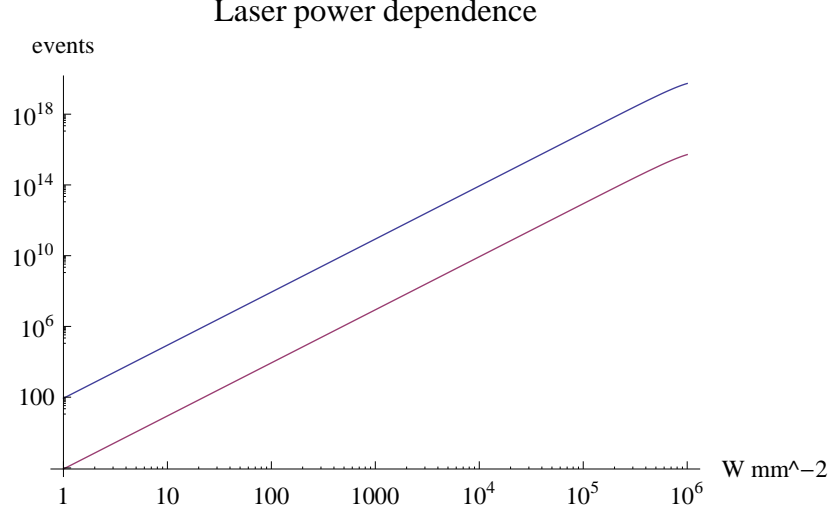


Figure 16: Rate at the arrival time of the target end as a function of laser power. Target number density 10^{16} (in blue), 10^{14}cm^{-3} (in purple), target length = 3 cm, laser duration 3 ns of 45 GHz, and $\theta_0 = \pi/4$ are assumed.

as 10^4cm^{-3} or even less, by taking into account a fast repetition cycle time of, for instance $O[\mu\text{sec}]$ ($O[10^6]$ times the event number of Fig(17) for the rate per second), whose precise value is determined by experimental conditions and not by a theoretical calculation. Dependence on the number density is roughly $\propto n^2$. This may open another interesting possibility of detecting PSR in alkali earth ions such as Ca^+ , Sr^+ and Ba^+ , which have the Λ -type level structure. The actual PSR rates, calculated by using experimentally known level spacings and decay rates for these ions, are somewhat smaller, as illustrated in Fig(18) for Ca^+ ion. Maintaining coherence in trapped ions might however be easier than in the gaseous phase. (Even production of the crystalized ion has been achieved.) A fast repetition cycle of excitation and trigger laser of order 1 msec might be quite sufficient to obtain detectable rates under good environment of the ion trap.

One might have a suspicion that PSR is not detectable, because a single photon SR rate is always larger than the two photon PSR rate due to a larger spontaneous emission rate, when both considered as elementary processes. This is not always true, because what should be compared in triggered experiments is the triggered PSR time vs the delay time of trigger-less SR, and these two times scale with the target number N as $\propto N^{-2}$ vs $\propto N^{-1}$. With a sufficiently large N , the triggered PSR occurs before the delayed SR occurs.

Incidentally, ($J=0 \rightarrow J=0$) PSR transitions, certainly present for alkali earth atoms (Sr, Ca etc.) and Yb, are very interesting from the point of realizing excellent quantum entanglement, because two emitted PSR photons are well entangled in their angular momenta, back to back emitted directions,

and identical photon energy, all to good accuracy.

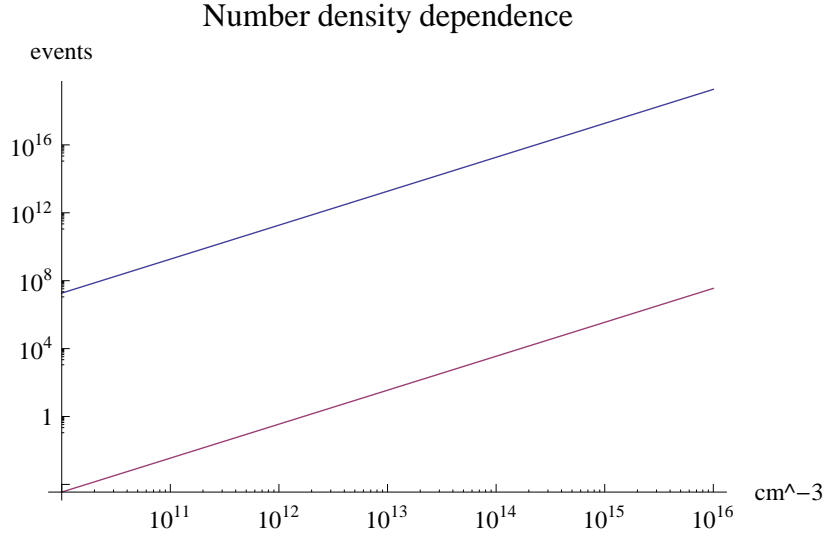


Figure 17: Rate at the arrival time of the target end as a function of Ba number density. Two power values 10^6 (in blue), 10^2W mm^{-2} (in purple), target length = 3 cm, laser duration 3 ns, $\theta_0 = \pi/4$ assumed.

Fig(19) shows a spectrum rate at a mistuned frequency of the input laser. Note that for an infinitely long medium the momentum and the energy conservation forces PSR spectrum to have a δ -function like peak at the half energy. In practice, the target has a finite length and violation of the momentum conservation leads to a small tail away from the peak location of $\omega = E_{eg}/2$. The amount of suppressed tail contribution depends much on the frequency distribution of the tail part of irradiated laser. A large suppression factor seen here is due to the Gaussian frequency distribution, in this case of width 45 GHz. This large suppression is encouraging from the point of enhancing the signal to the background ratio of RNPE/PSR. We shall have much more to say on this in the last section when we discuss prospects for RNPE.

We now demonstrate that solitons are stable against two photon emission. As discussed above, two photon emission associated with pulse propagation accompany simultaneously two photon absorption, since it may be induced by surrounding field. Thus, the net emission rate is in proportion to $R_3 I$, the product of population difference and the power of propagating pulse. For soliton solutions the time integrated rate at the target end is

$$\begin{aligned} & \int_{-\infty}^{\infty} dt \frac{2\alpha T'(t-L) (1 - \alpha^2(L - T(t-L))^2)}{(1 + \alpha^2(L - T(t-L))^2)^2} \\ &= 2 \int_{-\infty}^{\infty} dx \frac{1 - x^2}{(1 + x^2)^2} = 0. \end{aligned} \quad (80)$$

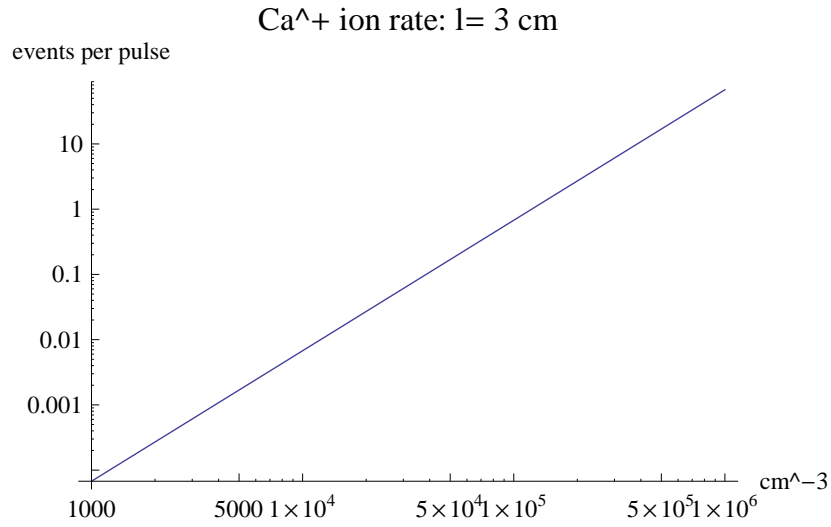


Figure 18: Rate for Ca⁺ ion vs number density. Power 10⁶W mm⁻², target length = 3 cm, laser duration 30 ns of 1 GHz width, $\theta_0 = \pi/4$ assumed.

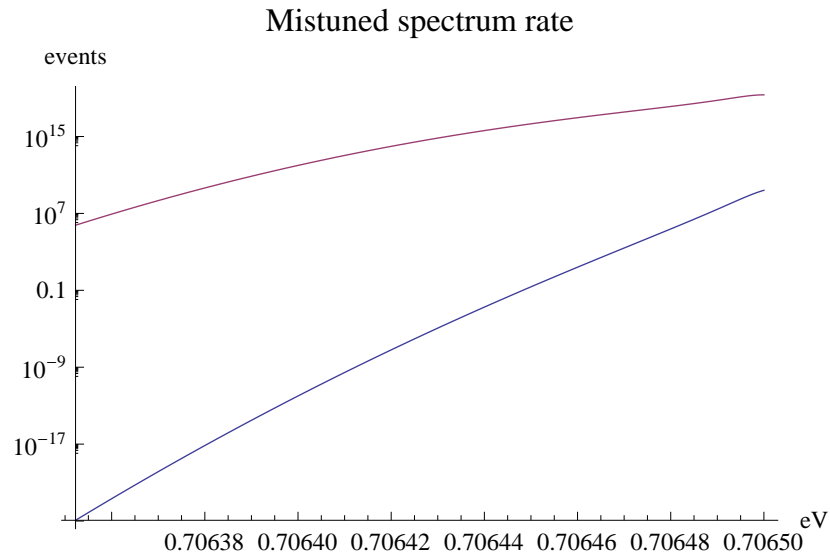


Figure 19: Photon spectrum in blue when the input laser frequency is mistuned by 10^{-4} away from the middle energy of $E_{eg}/2$. For comparison the original spectrum at the tuned frequency is also shown in purple.

From Fig(9) one sees that the emission region in the central part of the target is sandwiched by two absorption regions, which gives a balanced vanishing net rate. This result holds at any target point. In more general target states excluding solitons, the integral of this product $\propto \cos \theta \partial_t \theta$ gives a difference, $\sin \theta(t = \infty) - \sin \theta(t = -\infty)$, which is non-vanishing.

An ideal method of observing PSR might be creation of many solitons at the first stage, and their artificial destruction by controlled means for detection of PSR photons at the second stage.

The forward-backward asymmetry is expected to be large, both immediately prior to soliton formation and immediately after their destruction. We plot in Fig(20) time evolution of the asymmetric rates for $\sim 2\pi$ pulse. This asymmetry may be used to detect PSR itself under large symmetric backgrounds.

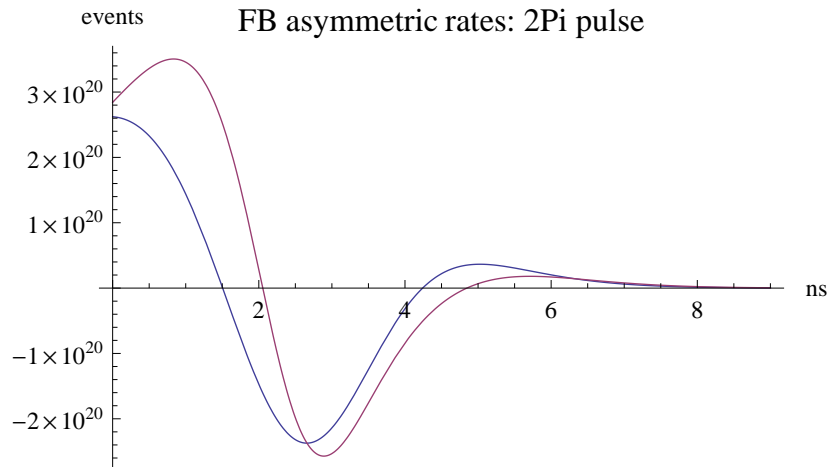


Figure 20: Forward-backward asymmetric PSR rates. The backward rate in blue is the measured rate at $x = 0$, and the forward rate in purple at $x = L$ (the target length 10 cm taken here). The rate here is (emission - absorption), hence the negative value region gives zero measurement. $\theta_0 = 0.9999 \times \pi$, and Ba number density 10^{16}cm^{-3} are assumed.

VII Outlook for radiative neutrino pair emission (RNPE)

We shall briefly sketch prospects towards our goal of the precision neutrino mass spectroscopy, by providing rate, spectrum and S/N. Details of rate computations, including effects of all six thresholds, mixing angles, Majorana vs Dirac distinction [4], and Majorana CP phases [5] shall be presented in a separate publication.

Atoms ideal for PSR may not be appropriate for RNPE detection, due to two reasons: (1) the

RNPE process $|e\rangle \rightarrow |g\rangle + \gamma + \nu_i \nu_j, i, j = 1, 2, 3$, requires a large spin flip amplitude [4] (similar to M1 transition for the electronic part of transition matrix element) between the intermediate state and either of the initial or the ground states, while a large PSR rate may require larger E1 transition, (2) PSR photons might become a serious background against RNPE, which means that smaller PSR rates are better for RNPE detection. To the best of our knowledge, Xe atom in solid form is among the best candidate atoms for RNPE. The candidate metastable state is the first excited state, $5p^5(^2P_{3/2})6s^2[3/2]_2$, a $J = 2$ pair state of electron and hole [5]. Other candidates might be metastable states of spin configuration (of two electrons) different from the ground state, commonly seen in diatomic molecules such as O_2 , an object worthy of serious consideration.

Experiments can be performed using typically more than three lasers of different frequencies; more than two for excitation to the metastable state and another for the trigger of RNPE. The trigger frequency ω (different from $E_{eg}/2$, hence mistuned for PSR) is reset each time for measurements at different photon energies of the RNPE continuous spectrum of Fig(21). Hence it is desirable to use frequency tunable lasers for the trigger. This way there is no Gaussian tail suppression at each detected spectral point of RNPE photon, while the background PSR is suppressed by the Gaussian tail factor due to a mismatch away from $\omega = E_{eg}/2$. Moreover, the energy resolution of RNPE photon is essentially determined by the precision of triggering laser frequency, and not by detected photon energy resolution. This is a key for success of the precision neutrino mass spectroscopy, which must resolve photon energies at the μeV level.

Theoretical estimates readily give coherent RNPE rates as large as, of order 0.1 events per pulse for Xe atoms of number density of order 10^{18}cm^{-3} , which may be realized in solid matrix environments. With a repetition cycle of $O[1]$ msec interval, this gives a detectable effective rate of $O[100]$ Hz. We show the continuous single photon energy spectrum of Xe macro-coherent RNPE in Fig(21). The sharp rise at the threshold is characteristic of the three-body decay under the momentum conservation, as is familiar in the μ decay. The increasing rate towards the low energy photon, given in the blue curve of Fig(21), is due to the flat frequency dependence of the peak intensity of the trigger laser, and the decreasing rate in purple is due to $\propto \omega^4$ peak intensity dependence more akin to the phase space of the 3-body spontaneous decay of elementary particles. The low energy side of the photon energy spectrum is thus sensitive to the frequency dependence of the trigger laser intensity, and is inevitably tied to experimental apparatus used. The rate scales as n^2V , with the target number density n and the volume V of coherent region, as shown in Fig(22).

The problem against the precision neutrino mass spectroscopy is not the rate itself, if a sufficient number of target atoms is prepared. Rather, the serious problem appeared to be in the signal to the background ratio (S/N) where the main background source is the physical process of two photon emission, in particular N^2 enhanced PSR. We discuss this problem shortly. Higher order QED processes that could sneak into our photon energy region might appear problematic, but they are

Compared RNPE rate per pulse: $n=10^{18} \text{ cm}^{-3}$, $l=10\text{cm}$

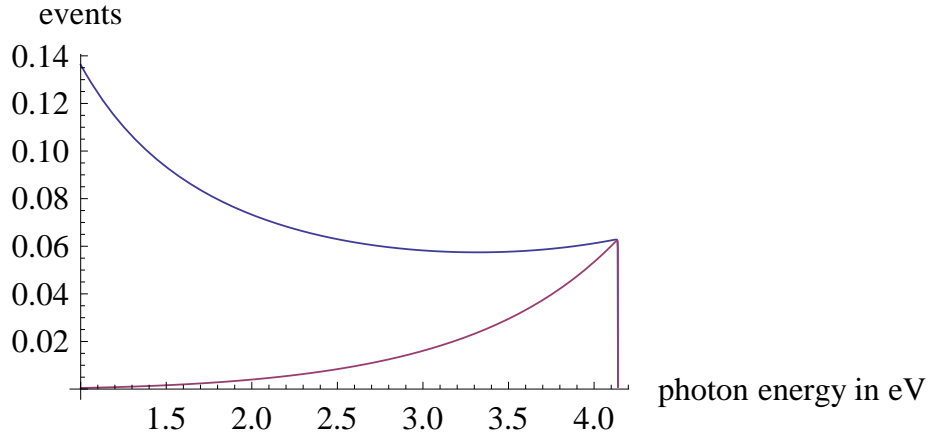


Figure 21: RNPE spectrum rate (event number per pulse) starting from the neutrino threshold of the pair of mass = 50 meV. Excited Xe number density = 10^{18} cm^{-3} . Two different frequency dependences of the laser peak intensity, the flat one (in blue) of magnitude 10^6 W mm^{-2} and the one $\propto \omega^4$ (in purple) are compared. Time duration = 3 ns. Complications due to mixing and phase factors, and to other thresholds are all ignored.

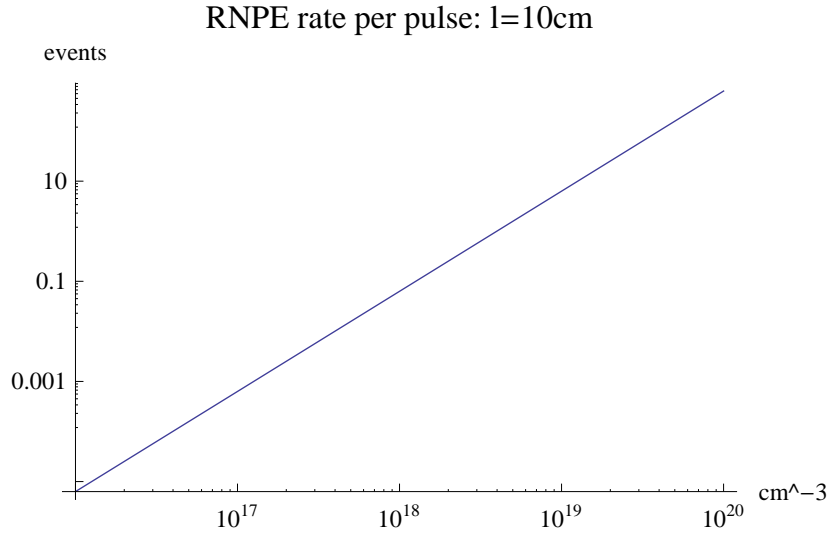


Figure 22: RNPE rate (event number per pulse) vs the target number density of pair emission of $m=1 \text{ meV}$ evaluated at $m=50 \text{ meV}$ pair threshold. Laser intensity 10^6 W mm^{-2} and time duration 3 ns are assumed.

actually negligible if they have (spontaneous) photon emission rates smaller than the elementary decay rate of metastable (lifetime $> O[1]$ msec in our standard) state, since in actual experiments a cycle of measurement for RNPE is terminated much earlier than the lifetime of metastable atom, and the target preparation is recycled. The single photon SR, entirely outside the photon energy region of our interest, is negligible also in rate by the choice of trigger frequency for RNPE.

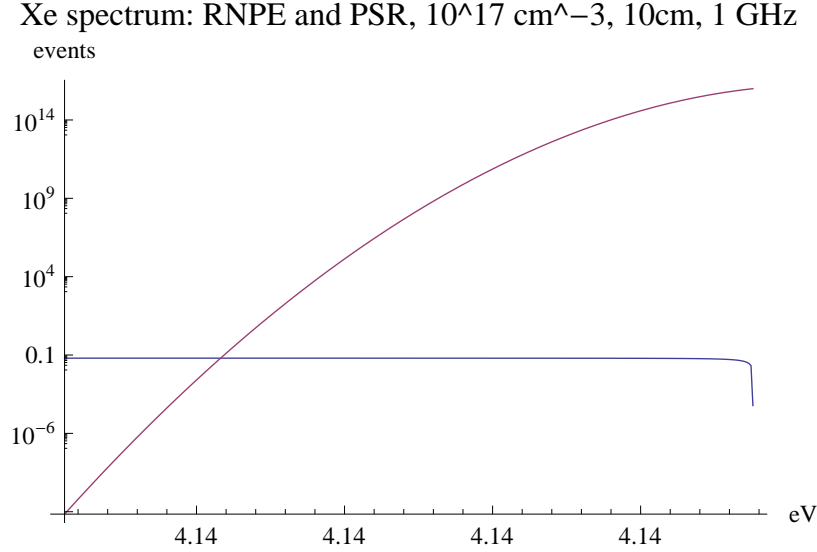


Figure 23: Rate of mass 1 meV pair emission (in blue) and the background PSR rate (in purple) very near the neutrino mass threshold. Excited Xe number density 10^{17}cm^{-3} of target length 10 cm and laser intensity 10^6W mm^{-2} of frequency width 1 GHz of time duration 30 ns are assumed. When the blue curve is above the purple curve, $S/N > 1$. At the farthest left is the threshold of the pair mass, $(8 + 1)$ meV, and at the farthest right is that of the pair mass, $(1 + 1)$ meV, the entire abscissa distance in this figure being separated by a very small energy interval $\sim 4.6\mu\text{eV}$ or ~ 7.1 GHz, hence their precise values are not shown.

As shown in the present paper, the S/N problem caused by PSR is much relaxed and the value of S/N is enormously enhanced by two effects; (1) mistuned trigger frequencies for PSR and (2) soliton formation. We first discuss the first issue. S/N is increased by the choice of trigger frequency set at $\omega \leq E_{eg}/2 - 2m_1^2/E_{eg}$ of the lightest neutrino pair emission for RNPE (we are ordering neutrino masses according to $m_3 > m_2 > m_1$). There is a mismatch of energy from the largest rate point at $\omega = E_{eg}/2$ of PSR by the amount $2m_1^2/E_{eg}$. If one may assume the Gaussian frequency distribution for the trigger laser, the PSR background rate is suppressed by a large factor of $\exp[-4m_1^4/(E_{eg}^2\delta^2)]$, with δ the Gaussian frequency width. A numerical factor of practical importance is $\sqrt{E_{eg}\delta}/2 \sim 1.2\text{meV}\sqrt{\delta/\text{GHz}}$. It is thus important to have the frequency width of sub-GHz in order to explore the sub-meV neutrino mass range.

In Fig(23) the spectral RNPE rate of assumed neutrino mass threshold is plotted, along with the background PSR rate, taking for the input laser 1 GHz frequency width of Gaussian distribution. It is estimated from this and similar figures of the pair mass range, $m_1 = (0.5 \sim 1)$, $m_2 = (8 \sim 10)$ meV, that this quality of laser can explore the neutrino mass of order 1 meV. With an even narrower width laser, one may hope to explore the sub-meV region and detection of the relic neutrino [9]. This, however, rests with the Gaussian nature of the tail part of the laser frequency distribution, which must be carefully examined from experimental points.

Soliton formation gives another great merit in which the background PSR is blocked, completely in ideal situations, and may open a new path towards a controlled RNPE experiment. In practice, only a partial blocking can be expected due to various kinds of relaxation processes. Naively, one would expect that the ratio of the relaxation to the soliton formation rate is a relevant quantity for the partial blocking. The soliton formation rate is however difficult to estimate without detailed experimental design and experimental R & D works. Study of decoherence in solid environments by means of detailed numerical simulation and R & D works is also very important for realization of the neutrino mass spectroscopy.

Acknowledgements

I should like to thank N. Sasao and members of SPAN experimental group for informative and helpful discussions on this subject.

VIII Appendix I Derivation of effective two level model

• Atomic system

The state vector of an atom can be expanded in terms of the wave function,

$$|\psi(t)\rangle = \sum_j c_j(t)e^{-iE_j t}|j\rangle + c_g(t)e^{-iE_g t}|g\rangle + c_e(t)e^{-iE_e t}|e\rangle. \quad (81)$$

$c_\alpha(t)$ are probability amplitudes in an interaction picture.

The atomic system may interact with fields. The electric field $\epsilon(x, t)$ that appears in the Hamiltonian via E1 or M1 transition is assumed to have one component alone, namely we ignore effects of field polarization. This is a valid approach under a number of circumstances. One then decomposes the real field variable $\epsilon(x, t)$ into Fourier series, $e^{i\omega t}$ times a complex envelope amplitude $E_0(x, t)$, and its conjugate, where $E_0(x, t)e^{ikx}$ ($k =$ wave number) is assumed slowly varying in time,

$$\epsilon(x, t) = E_0(x, t)e^{i\omega t} + E_0^*(x, t)e^{-i\omega t}. \quad (82)$$

The Schrödinger equation for a single atom

$$i\frac{\partial}{\partial t}|\psi(t)\rangle = (H_0 + d\epsilon)|\psi(t)\rangle, \quad (83)$$

gives the upper level amplitude $c_j(t)$. Using

$$i\frac{\partial}{\partial t}\langle j|\psi(t)\rangle = \langle j|(H_0 + d\epsilon)|\psi(t)\rangle, \quad (84)$$

one has

$$i\frac{dc_j}{dt}e^{-iE_j t} = (d_{je}c_e e^{-iE_e t} + d_{jg}c_g e^{-iE_g t})\epsilon. \quad (85)$$

This can formally be integrated to

$$\begin{aligned} c_j(t) &= -i \int_0^t dt' \left(d_{je}\epsilon(x, t')c_e(t')e^{i(E_j - E_e)t'} + d_{jg}\epsilon(x, t')c_g(t')e^{i(E_j - E_g)t'} \right) \\ &= -i \int_0^t dt' \left(d_{je}c_e(t')e^{iE_{je}t'} + d_{jg}c_g(t')e^{iE_{jg}t'} \right) \left(E_0(x, t')e^{i\omega t'} + E_0^*(x, t')e^{-i\omega t'} \right), \end{aligned} \quad (86)$$

(the initial condition $c_j(0) = 0$ is assumed).

We extend the system of a single atom to a collection of atoms, regarding variables $c_\alpha(x, t)$ as functions of two variables, x and t . The population and the coherence of the entire atomic system is described by the density matrix elements, $R_{\alpha\beta}(x, t)$, $\alpha\beta = e, g, j$, which is the squared product of wave functions (bilinears in c_e, c_g, c_j and their conjugates) and the target number density $n(x)$. The macro-variables are defined by

$$R_{\alpha\beta}(x, t) = n(x)c_\alpha^*(x, t)c_\beta(x, t). \quad (87)$$

For a notational simplicity we often omit space coordinate (x) dependence of probability amplitudes and write these simply as $c_\alpha(t)$ instead of more proper $c_\alpha(x, t)$.

• Markovian approximation and SVEA

The basic strategy of deriving equations for the lower two level amplitudes c_e, c_g in a closed form is to eliminate atomic variables related to the upper level amplitude c_j . This is essentially done by neglecting a long-time memory effect (the Markovian approximation) and making slowly varying envelope approximation (SVEA) in the terminology of [3]. The idea is to replace dynamical variables, $c_e(t'), c_g(t'), E(x, t')$ in the integrand of eq.(86), by their values at time t , neglecting all the past memory effects. This gives

$$\begin{aligned} c_j(t) &\approx d_{je}c_e \left(\frac{1 - e^{i(\omega + E_{je})t}}{\omega + E_{je}} E_0 - \frac{1 - e^{-i(\omega - E_{je})t}}{\omega - E_{je}} E_0^* \right) \\ &+ d_{jg}c_g \left(\frac{1 - e^{i(\omega + E_{jg})t}}{\omega + E_{jg}} E_0 - \frac{1 - e^{-i(\omega - E_{jg})t}}{\omega - E_{jg}} E_0^* \right), \end{aligned} \quad (88)$$

which is inserted into equations for the lower levels

$$\frac{dc_e}{dt} = -i \sum_j d_{ej} \epsilon(x, t) c_j(t) e^{iE_{ej}t}, \quad (89)$$

$$\frac{dc_g}{dt} = -i \sum_j d_{gj} \epsilon(x, t) c_j(t) e^{iE_{gj}t}. \quad (90)$$

Unitarity, namely the probability conservation, given by

$$\frac{d}{dt} (|c_e|^2 + |c_g|^2 + \sum_j |c_j|^2) = 0, \quad (91)$$

does not hold when limited to two amplitudes c_e, c_g alone, namely in the Markovian approximation. However there exists an effective conservation law that holds for the two level system, given later by (114). There seems some misunderstanding on this point in [3].

We further neglect rapidly oscillating terms assuming the nearly, but not necessarily exactly, tuned condition, $\omega \approx E_{eg}/2$, which amounts to

$$\frac{dc_e}{dt} = i (\mu_{ee} |E_0^2| c_e(t) + \mu_{eg} (E_0^*)^2 c_g(t) e^{-i(2\omega - E_{eg})t}), \quad (92)$$

$$\frac{dc_g}{dt} = i (\mu_{gg} |E_0^2| c_g(t) + \mu_{ge} E_0^2 c_e(t) e^{i(2\omega - E_{eg})t}), \quad (93)$$

$$\mu_{ee} = 2 \sum_j \frac{d_{je}^2 E_{je}}{E_{je}^2 - \omega^2}, \quad \mu_{gg} = 2 \sum_j \frac{d_{jg}^2 E_{jg}}{E_{jg}^2 - \omega^2}, \quad (94)$$

$$\mu_{eg} = \sum_j \frac{d_{je} d_{jg}}{E_c - \delta\omega}, \quad \mu_{ge} = \sum_j \frac{d_{je} d_{jg}}{E_c + \delta\omega}, \quad (95)$$

where $E_c = \frac{1}{2}(E_{jg} + E_{je})$, $\delta\omega = \omega - \frac{E_{eg}}{2}$ as in the text. All of $d_{j\alpha}, \mu_{\alpha\beta}$ are taken as real.

A mistake in [3] is that $\mu_{eg} = \mu_{ge}$ is assumed even at $\delta\omega \neq 0$. This equality holds only at the middle point of frequency $\omega = E_{eg}/2$. Thus, results of [3] away from this tuned frequency should be taken with skepticism.

Writing this equation in a matrix form,

$$\frac{d}{dt} \begin{pmatrix} c_e \\ c_g \end{pmatrix} = -i\mathcal{H} \begin{pmatrix} c_e \\ c_g \end{pmatrix}, \quad (96)$$

$$\mathcal{H} = \begin{pmatrix} \mu_{ee} |E_0^2| & e^{-i(2\omega - E_{eg})t} \mu_{eg} (E_0^*)^2 \\ e^{i(2\omega - E_{eg})t} \mu_{ge} E_0^2 & \mu_{gg} |E_0^2| \end{pmatrix}, \quad (97)$$

one finds that the effective Hamiltonian \mathcal{H} becomes hermitian only by neglecting $\delta\omega/E_c$ terms in μ_{eg}, μ_{ge} .

We introduce symmetric and anti-symmetric functions of $\delta\omega = \omega - E_{eg}/2$ as

$$\mu^+ = \sum_j \frac{d_{je}d_{jg}E_c}{E_c^2 - \delta\omega^2}, \quad \mu^- = \sum_j \frac{d_{je}d_{jg}\delta\omega}{E_c^2 - \delta\omega^2}, \quad (98)$$

$$\mu_{eg} = \mu^+ + \mu^-, \quad \mu_{ge} = \mu^+ - \mu^-, \quad (99)$$

and write

$$\mathcal{H} = \mathcal{H}^+ + \mathcal{H}^-, \quad (100)$$

$$\mathcal{H}^+ = \begin{pmatrix} \mu_{ee}|E_0^2| & e^{-i(2\omega-E_{eg})t}\mu^+(E_0^*)^2 \\ e^{i(2\omega-E_{eg})t}\mu^+E_0^2 & \mu_{gg}|E_0^2| \end{pmatrix}, \quad (101)$$

$$\mathcal{H}^- = \begin{pmatrix} 0 & e^{-i(2\omega-E_{eg})t}\mu^-(E_0^*)^2 \\ -e^{i(2\omega-E_{eg})t}\mu^-E_0^2 & 0 \end{pmatrix}. \quad (102)$$

\mathcal{H}^+ is hermitian, while \mathcal{H}^- is anti-hermitian. The anti-symmetric piece \mathcal{H}^- vanishes at the middle point of $\delta\omega = 0$, since $\mathcal{H}^- \propto \mu^- \propto \delta\omega$, hence is small except where $\delta\omega$ is large of $O[E_c]$. We shall ignore effect of \mathcal{H}^- and assume $\mu_{ge} = \mu_{eg}$ in the main text of the present work.

• Generalized Bloch vector and its dynamical equation

The 4 component Bloch vector is defined by

$$R_0 = n(|c_e|^2 + |c_g|^2), \quad (103)$$

$$R_1 = in(c_g^*c_e e^{in} - c_e^*c_g e^{-in}), \quad (104)$$

$$R_2 = -n(c_g^*c_e e^{in} + c_e^*c_g e^{-in}), \quad (105)$$

$$R_3 = n(|c_e|^2 - |c_g|^2), \quad (106)$$

$$\eta = (2\omega - E_{eg})t - 2kx + 2\varphi, \quad (107)$$

where we assume a standard form of field,

$$\epsilon(x, t) = \epsilon_0(x, t) \cos(\omega t - kx + \varphi), \quad (108)$$

with $k = \pm\omega$. The real amplitude $\epsilon_0(x, t)$ and the phase $\varphi(x, t)$ are assumed both slowly varying in time and in space. Note the relation of real and complex field, $\epsilon_0^2 = 4|E_0|^2$ (E_0 is complex including $e^{i(\omega t - kx)}$).

The generalized Bloch equation is given by

$$\frac{\partial}{\partial t} R_1 = \left(\frac{\mu_{ee} - \mu_{gg}}{4} \epsilon_0^2 + (2\omega - E_{eg} + 2\frac{\partial\varphi}{\partial t}) \right) R_2 + \frac{\mu^+}{2} \epsilon_0^2 R_3 - \frac{\mu^-}{2} \epsilon_0^2 R_0, \quad (109)$$

$$\frac{\partial}{\partial t} R_2 = - \left(\frac{\mu_{ee} - \mu_{gg}}{4} \epsilon_0^2 + (2\omega - E_{eg} + 2\frac{\partial\varphi}{\partial t}) \right) R_1, \quad (110)$$

$$\frac{\partial}{\partial t} R_3 = -\frac{\mu^+}{2} \epsilon_0^2 R_1, \quad (111)$$

$$\frac{\partial}{\partial t} R_0 = \frac{\mu^-}{2} \epsilon_0^2 R_1, \quad (112)$$

$$\mu^+ = \sum_j \frac{d_{ej} d_{gj} E_c}{E_c^2 - (\omega - E_{eg}/2)^2}, \quad (113)$$

proved by using the Schrödinger equation for c_e, c_g . Note that in RHS of these equations there is no phase factor like $e^{i(2kt-2\omega t+E_{eg}t)}$.

The conservation law is extended to the 4-vector;

$$\frac{\partial}{\partial t} (R_0^2 + R_1^2 + R_2^2 + R_3^2) = 0. \quad (114)$$

Only at the middle point of $\omega = E_{eg}/2$ this conservation reduces to the usual type of conservation for the 3-vector norm, $\frac{\partial}{\partial t} (R_1^2 + R_2^2 + R_3^2) = 0$ (the assumption taken in [3]), since in this case $\mu^- = 0$ and one has separately $\partial_t R_0^2 = 0$.

• Polarization of medium

Polarization vector is defined by

$$P = n(x) \langle \psi(t) | d | \psi(t) \rangle = n \sum_j (d_{ej} c_e^* c_j e^{-iE_{je}t} + d_{gj} c_g^* c_j e^{-iE_{jg}t} + \text{c.c.}), \quad (115)$$

for which we eliminate c_j using eq.(88).

The polarization can be decomposed into the in-phase $\cos(\omega t - kx + \varphi)$ and the out-phase $\sin(\omega t - kx + \varphi)$ parts;

$$\begin{aligned} P &= n(x) (\mu_{ee} |c_e|^2 + \mu_{gg} |c_g|^2 - (\mu_{eg} c_g c_e^* e^{-i\eta} + \mu_{ge} c_g^* c_e e^{i\eta})) \epsilon_0(x, t) \cos(\omega t - kx + \varphi) \\ &\quad - i(\mu_{eg} c_g c_e^* e^{-i\eta} - \mu_{ge} c_g^* c_e e^{i\eta}) \epsilon_0(x, t) \sin(\omega t - kx + \varphi) \\ &= \left(\frac{\mu_{ee} + \mu_{gg}}{2} n + \frac{\mu_{ee} - \mu_{gg}}{2} R_3 + \mu^+ R_2 \right) \epsilon_0(x, t) \cos(\omega t - kx + \varphi) + \mu^+ R_1 \epsilon_0(x, t) \sin(\omega t - kx + \varphi). \end{aligned} \quad (116)$$

$O[\mu^-]$ terms do not contribute to hermitian polarization P .

The Maxwell equation

$$\left(\frac{\partial^2}{\partial x^2} - \frac{\partial^2}{\partial t^2} \right) \epsilon = \frac{\partial^2 P}{\partial t^2}, \quad (117)$$

gives for envelope amplitude and phase variation under SVEA

$$(\partial_t + \partial_x)\epsilon_0^2 = \omega\mu^+\epsilon_0^2R_1, \quad (118)$$

$$(\partial_t + \partial_x)2\varphi = \omega \left(-\omega\mu^+R_2 + \frac{\mu_{ee} - \mu_{gg}}{2}R_3 + \frac{\mu_{ee} + \mu_{gg}}{2}n \right). \quad (119)$$

In order to simplify equations, we introduce new variables by

$$R'_2 = \frac{R_2 - \gamma R_3}{\sqrt{1 + \gamma^2}}, \quad R'_3 = \frac{\gamma R_2 + R_3}{\sqrt{1 + \gamma^2}}, \quad (120)$$

$$\omega_R = \frac{\sqrt{1 + \gamma^2}}{2}\mu^+\epsilon_0^2, \quad (121)$$

$$\gamma = \frac{\mu_{ee} - \mu_{gg}}{2\mu^+}, \quad \Omega = 2\omega - E_{eg} + 2\frac{\partial\varphi}{\partial t}. \quad (122)$$

The basic set of equations is given by

$$\partial_t R_1 = \omega_R R'_3 + \frac{\Omega}{\sqrt{1 + \gamma^2}}(R'_2 + \gamma R'_3) - \frac{\mu^-}{2}\epsilon_0^2 R_0, \quad (123)$$

$$\partial_t R'_2 = -\frac{\Omega}{\sqrt{1 + \gamma^2}}R_1, \quad (124)$$

$$\partial_t R'_3 = -\omega_R R_1 - \frac{\gamma\Omega}{\sqrt{1 + \gamma^2}}R_1, \quad (125)$$

$$\partial_t R_0 = \frac{\mu^-}{2}\epsilon_0^2 R_1, \quad (126)$$

$$(\partial_t + \partial_x)\omega_R + \kappa\omega_R = \omega\mu^+\omega_R R_1, \quad (127)$$

$$(\partial_t + \partial_x)\Omega = 2\omega\mu^+R_1\Omega, \quad (128)$$

from which it follows

$$\partial_t (R_0^2 + R_1^2 + (R'_2)^2 + (R'_3)^2) = 0. \quad (129)$$

We have not included atomic relaxation effects given by parameters, T_1, T_2, T_2^* [1].

One can consistently take $\Omega = 0$, namely $\partial_t\varphi = E_{eg}/2 - \omega$. This adjustment of field phase is assumed in the text of this paper.

For both $\mu^- = 0$ and $\Omega = 0$ the system further simplifies to eqs.(15), (16) and (18) in the text by an appropriate choice of variables.

IX Appendix II Details towards construction of analytic solutions

We start from discussions that lead to introduction of the tipping angle $\theta(x, t)$, eq.(17), related to the Bloch vector component by $R_3 \propto \cos\theta$. Another important relation (18), $\partial_t\theta \propto |E_0^2|$, gives a physical content of the area function θ , relating it to an integral of the pulse flux $|E_0^2|$.

Our method for solving non-linear partial differential equations of two independent variables (x and t) is to integrate in one variable t and replace integration constants obtained this way by functions including another variable x . The method works for our problem of one mode propagation, but it is not a general mathematical method.

At finite time t we allow the integration constant t_0, θ_0 of 0d solution (solution without space dependence), eq.(27), to vary in spacetime according to

$$t_0 \rightarrow T(t-x), \quad \theta_0 \rightarrow \theta_p(x), \quad (130)$$

$$(\partial_t + \partial_x)\theta + \alpha(\cos \theta - \cos \theta_p) = 0, \quad (131)$$

noting a trivial equality, $(\partial_t + \partial_x)T(t-x) = 0$. Hence, solutions are written in terms of two functions to be determined by the initial and the boundary data,

$$\theta(x, t) = \arccos \frac{\cos \theta_p(x) \cosh(\alpha(t - T(t-x)) \sin \theta_p) - 1}{\cosh(\alpha(t - T(t-x)) \sin \theta_p) - \cos \theta_p(x)}, \quad (132)$$

$$\omega_R(x, t) = \partial_t \theta = \frac{-\alpha(1 - \partial_t T(t-x)) \sin^2 \theta_p(x)}{\cosh(\alpha(t - T(t-x)) \sin \theta_p) - \cos \theta_p(x)}, \quad (133)$$

where $\theta_p(x), T(y = t-x)$ are yet to be determined.

The following, somewhat complicated steps leading to eqs.(137) and (140) are processes of how the initial and the boundary conditions determine the unknown functions, $\theta_p(x), T(y)$.

The given boundary data at some spatial point $x = 0$, the target end at which laser irradiation takes place, and the initial data at $t = 0$ are

$$\theta(x = 0, t) \equiv \tilde{\theta}(t), \quad \theta(x, t = 0). \quad (134)$$

These are related to the variable $\omega_R(x, t)$ by using $\partial_t \theta(x, t) = \omega_R(x, t)$,

$$\theta(0, t) = \int_{-\infty}^t dt' \omega_R(0, t'), \quad (135)$$

$$\theta(x, 0) = \int_{-\infty}^0 dt' \omega_R(x, t'). \quad (136)$$

Note that two data (134) are independent.

We may solve for the unknown function $T(\tau)$ using the boundary condition, to get

$$T(\tau) = \tau - \frac{1}{\alpha \sin \theta_0} \operatorname{arccosh} \frac{1 - \cos \theta_0 \cos \tilde{\theta}(\tau)}{\cos \theta_0 - \cos \tilde{\theta}(\tau)}, \quad \theta_0 \equiv \theta_p(0). \quad (137)$$

The solution for $\theta_p(x)$ is obtained from the initial condition, given by

$$\partial_t \tilde{\theta}(-x)(\cos \theta_p - \cos \theta(x, 0)) = (\cos \theta_0 - \cos \tilde{\theta}(-x)) \omega_R(x, 0). \quad (138)$$

This equation together with eq.(133) calculated at $t = 0, x = 0$ and (137), gives, with $\tilde{\mu} \equiv \sqrt{(\mu_{gg} - \mu_{ee})^2 + 4\mu_{ge}^2}/4$,

$$\cos \theta(0, 0) = \pm \cos \tilde{\theta}(0), \quad \tilde{\theta}(0) = \tilde{\mu} \int_{-\infty}^0 dy |\epsilon_0^2(y)|, \quad (139)$$

+(-) corresponding to amplifier (absorber). The second equation of (139) is derived from the area-intensity relation, $\partial_t \tilde{\theta} \propto |\epsilon_0^2|$, for the incident pulse.

If the major part of input laser is still far away from the target end of $x = L$, $\tilde{\theta}(0) \approx 0$, and $\theta(0, 0) \approx 0$ (π). The amplifier case of $\theta(0, 0) \approx 0$ corresponds to a physical situation in which medium is excited by other lasers, while the absorber case of $\theta(0, 0) \approx \pi$ to medium in the ground state.

Equation (133) calculated at other points of $t = 0$ gives

$$\cos \theta(x, 0) = \cos \theta_p(x) - \frac{\sin^2 \theta_p(x)}{\cosh(\alpha T(-x) \sin \theta_p(x)) - \cos \theta_p(x)}. \quad (140)$$

Since $T(-x)$ here is already given in terms of $\tilde{\theta}(-x)$ by eq.(137), this equation determines $\cos \theta_p(x)$ in terms of the initial data $\cos \theta(x, 0)$. We find it possible to construct solutions of these equations only when $\theta_p(x) = \theta_0$ (spatially constant).

Explicit form of solution is then ($0 \leq \theta_0 \leq \pi$)

$$|E_0^2(x, t)| = \frac{\sin^2 \theta_0 |\epsilon_0^2(t-x)|}{\cosh(\alpha x \sin \theta_0)(1 - \cos \theta_0 \cos \tilde{\theta}) \pm \sinh(\alpha x \sin \theta_0) \sin \theta_0 \sin \tilde{\theta} - \cos \theta_0 (\cos \theta_0 - \cos \tilde{\theta})}, \quad (141)$$

$$\cos \theta(x, t) = \mp \frac{\cosh(\alpha x \sin \theta_0) \cos \theta_0 (1 - \cos \theta_0 \cos \tilde{\theta}) \pm \sinh(\alpha x \sin \theta_0) \cos \theta_0 \sin \theta_0 \sin \tilde{\theta} - (\cos \theta_0 - \cos \tilde{\theta})}{\cosh(\alpha x \sin \theta_0)(1 - \cos \theta_0 \cos \tilde{\theta}) \pm \sinh(\alpha x \sin \theta_0) \sin \theta_0 \sin \tilde{\theta} - \cos \theta_0 (\cos \theta_0 - \cos \tilde{\theta})}, \quad (142)$$

$$R_3(x, t) = \frac{n}{\sqrt{1 + \gamma^2}} \cos \theta(x, t), \quad (143)$$

with variable dependence given by x explicitly and $t - x$ in $\tilde{\theta}(t - x)$. These solutions are given in terms of the strength of input pulse,

$$\tilde{\theta}(t - x) = \tilde{\mu} \int_{-\infty}^{t-x} dy |\epsilon_0^2(y)|. \quad (144)$$

The constraint $\cos^2 \theta(x, t) \leq 1$ is satisfied for any θ_0 .

Note that $\tilde{\theta}$ is monotonically increasing function of its argument. The solution $\theta(x, t)$ is valid only for $\partial_t \theta > 0$ for the positivity of the pulse strength.

We do not know whether these solutions have complete generality and no other solutions exist, but they seem to be adequately general for our purposes. The initial data $\theta(x, 0)$ at $x > 0$ consistent with these solutions is given in terms of the input area at negative arguments $\tilde{\theta}(-x)$, and they are

independent of the boundary data $\theta(0, t)$ at $t > 0$ given by the same area of positive arguments. One might consider the situation of $\tilde{\theta}(-x) = 0$ at $x > 0$, which gives

$$\cos \theta(x, 0) = \frac{\cos \theta_0 \cosh(\alpha x \sin \theta_0) + 1}{\cosh(\alpha x \sin \theta_0) + \cos \theta_0}, \quad (145)$$

References

- [1] For an excellent review of both the theory and experiments of superradiance, M. Benedict, A.M. Ermolaev, V.A. Malyshev, I.V. Sokolov, and E.D. Trifonov, *Super-radiance Multiatomic coherent emission*, Informa (1996).
- For a formal aspect of the theory, M. Gross and S. Haroche, *Phys.Rep.***93**, 301(1982).
- The original suggestion of superradiance is due to R.H. Dicke, *Phys. Rev.***93**, 99(1954).
- [2] M. Yoshimura, C. Ohae, A. Fukumi, K. Nakajima, I. Nakano, H. Nanjo, and N. Sasao, *Macro-coherent two photon and radiative neutrino pair emission*, arXiv 805.1970[hep-ph](2008).
- M. Yoshimura, *Neutrino Spectroscopy using Atoms (SPAN)*, in Proceedings of 4th NO-VE International Workshop, edited by M. Baldo Ceolin(2008).
- [3] L.M. Narducci et al., *A Model of Degenerate Two-photon Amplifier*, in *Cooperative Effects in Matter and Radiation*, ed. by C.M. Bowden, D.W. Howgate, and H.R. Robl Prentice Hall, New York (1977); L.M. Narducci, W.W. Eidson, P. Furcinitti, and D.C. Eteson, *Phys. Rev.***A 16**, 1665 (1977).
- [4] M. Yoshimura, *Phys. Rev.***D75**, 113007(2007).
- [5] M. Yoshimura, A. Fukumi, N. Sasao and T. Yamaguchi, *Progr. Theor. Phys.***123**, 523(2010), and *Parity violating observables in radiative neutrino pair emission from metastable atoms*, arXiv:0907.0519v2 [hep-ph] (2009).
- [6] S.L. McCall and E.L. Hahn, *Phys. Rev.***183**, 457(1969).
- For a review, L. Allen and J.H. Eberly, *Optical Resonance and Two-level Atoms*, Dover, New York, (1975).
- For comparison with experimental results, R.E. Slusher and H.M. Gibbs, *Phys. Rev.***A4**, 1634(1972).

- [7] For examples, B.H. Bransden and C.J. Joachain, *Physics of Atoms and Molecules*, 2nd edition, Prentice Hall (2003); D. Budker, D.F. Kimball and D.P. DeMille, *Atomic Physics*, Oxford University Press, New York (2004).
- [8] For a review, C. Cohen-Tannoudji, J. Dupont-Roc, and G. Grynberg, *Atom-Photon Interactions*, Wiley-VCH(2004).
- [9] T. Takahashi and M. Yoshimura, *Effect of Relic Neutrino on Neutrino Pair Emission from Metastable Atoms*, hep-ph/0703019.